JCTC Journal of Chemical Theory and Computation

Article

pubs.acs.org/JCTC

# Assessment of Approximate Coupled-Cluster and Algebraic-Diagrammatic-Construction Methods for Ground- and Excited-State Reaction Paths and the Conical-Intersection Seam of a Retinal-Chromophore Model

Deniz Tuna,[*,†] Daniel Lefrancois,[‡] Łukasz Wolański,[§] Samer Gozem,[∥] Igor Schapiro,[⊥,▽] Tadeusz Andruniów,[*,§] Andreas Dreuw,[*,‡] and Massimo Olivucci[*,#,○]

[†]Max-Planck-Institut für Kohlenforschung, 45470 Mülheim an der Ruhr, Germany

[‡]Interdisciplinary Center for Scientific Computing, University of Heidelberg, 69120 Heidelberg, Germany

[§]Department of Chemistry, Wrocław University of Technology, 50370 Wrocław, Poland

[∥]Department of Chemistry, University of Southern California, Los Angeles, California 90089, United States

[⊥]Institut de Physique et Chimie des Matériaux de Strasbourg & Labex NIE, Université de Strasbourg, CNRS UMR 7504, Strasbourg 67034, France

[#]Department of Chemistry, Bowling Green State University, Bowling Green, Ohio 43402, United States

[○]Dipartimento di Biotecnologie, Chimica e Farmacia, Universitá de Siena, 53100 Siena, Italy

Supporting Information

**ABSTRACT:** As a minimal model of the chromophore of rhodopsin proteins, the penta-2,4-dieniminium cation (PSB3) poses a challenging test system for the assessment of electronic-structure methods for the exploration of ground- and excited-state potential-energy surfaces, the topography of conical intersections, and the dimensionality (topology) of the branching space. Herein, we report on the performance of the approximate linear-response coupled-cluster method of second order (CC2) and the algebraic-diagrammatic-construction scheme of the polarization propagator of second and third orders (ADC(2) and ADC(3)). For the ADC(2) method, we considered both the strict and extended variants (ADC(2)-s and ADC(2)-x). For both CC2 and ADC methods, we also tested the spin-component-scaled (SCS) and spin-opposite-scaled (SOS) variants. We have explored several ground- and excited-state reaction paths, a circular path centered around the $S_1/S_0$ surface crossing, and a 2D scan of the potential-energy surfaces along the branching space. We find that the CC2 and ADC methods yield a different dimensionality of the intersection space. While the ADC methods yield a linear intersection topology, we find a conical intersection topology for the CC2 method. We present computational evidence showing that the linear-response CC2 method yields a surface crossing between the reference state and the first response state featuring characteristics that are expected for a true conical intersection. Finally, we test the performance of these methods for the approximate geometry optimization of the $S_1/S_0$ minimum-energy conical intersection and compare the geometries with available data from multireference methods. The present study provides new insight into the performance of linear-response CC2 and polarization-propagator ADC methods for molecular electronic spectroscopy and applications in computational photochemistry.

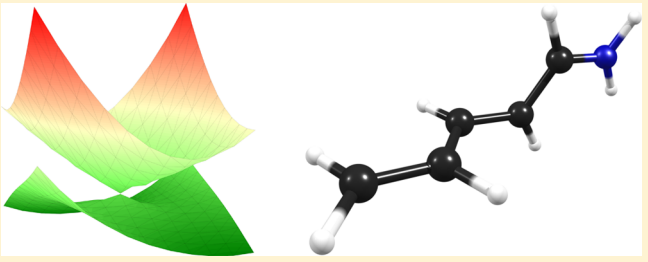

## 1. INTRODUCTION

The penta-2,4-dieniminium cation (PSB3) has been extensively used as a minimal model system of the protonated Schiff base of retinal (rPSB), which is the chromophore of light-sensitive rhodopsin proteins (cf. Figure 1). In vertebrate and invertebrate retinas or in microbial membranes, the photoisomerization of rhodopsins initiates a reaction cascade that lies at the heart of light-sensing and other light-driven functions throughout various unicellular (archaea, eubacteria, and eukaryotic microbes) and multicellular (invertebrate and vertebrate) organisms. Static calculations, that is, the computation of vertical excitation energies, the optimization of excited-state equilibrium geometries and minimum-energy conical intersections, and the mapping of excited-state potential-energy surfaces and conical-intersection seams, have been performed on PSB3 for almost two decades.[1−16] Insight into the photoinduced dynamics of PSB3 has been gained by performing nonadiabatic molecular-dynamics simulations on the isolated and solvated forms.[17−26]

**Received:** January 12, 2015
**Published:** October 22, 2015






DOI: 10.1021/acs.jctc.5b00022
J. Chem. Theory Comput. 2015, 11, 5758−5781

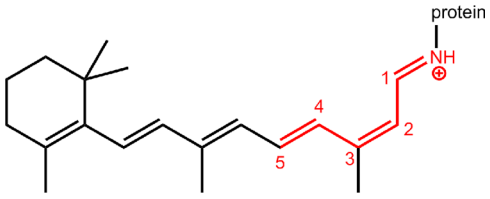


**Figure 1.** Structural formulas of the 13-*cis* rPSB chromophore of microbial rhodopsins (large structure) and of the model system PSB3 (red substructure, for which the bond to the protein is substituted by a hydrogen atom). The numbering shown for PSB3 is used throughout this article.

In recent years, we have conducted a series of extensive benchmark studies for testing various *ab initio* and density-functional theory methods with respect to their performance in describing the potential-energy surfaces of the electronic ground state and the first electronically excited singlet state driving the photoisomerization of the central double bond of PSB3. Particular attention was paid to the performance of these methods in describing the potential-energy surfaces and associated electronic wave functions in the vicinity of a conical intersection and its topography and topology along the branching space. Methods that have been tested so far include CASSCF, CASPT2, MRCISD(+Q), NEVPT2, XMCQDPT2, EOM-CC, SORCI, and quantum Monte Carlo as well as several methods based on density-functional theory.[27−34] Herein, we extend this benchmark series to the linear-response approximate coupled-cluster (CC) method of second order (CC2) and to the algebraic-diagrammatic-construction (ADC) method of the polarization propagator of second and third orders (ADC(2) and ADC(3)). For the ADC(2) method, we considered both the strict (ADC(2)-s) and extended (ADC(2)-x) variants, and for both CC2 and ADC methods, we also considered the spin-component-scaled (SCS) and spin-opposite-scaled (SOS) variants. The present contribution carries forward an ongoing effort to identify and assess computational methods for a balanced description of both molecular electronic spectroscopy and photochemical processes.[35−37]

The approximate coupled-cluster method of second order (CC2) was formulated by Christiansen, Koch, and Jørgensen as an approximation of the CCSD method, which reduces the scaling of the computational effort from $N^6$ for CCSD to $N^5$ for CC2, with $N$ being the number of one-electron basis functions.[38] A few years later, an efficient code, which makes use of the resolution-of-the-identity (RI) approximation and the linear-response formalism for the computation of electronically excited states, was implemented into the program package Turbomole[39] by Hättig and Weigend.[40] Köhn and Hättig then developed analytical excited-state gradients,[41,42] transition moments, and molecular properties[43] for the CC2 method. Other quantum-chemistry programs that provide the CC2 method are Dalton,[44] CFOUR,[45] Psi-4,[46] Molpro,[47] and NWChem.[48] Due to its high efficiency, linear-response RI-CC2 has been extensively used for the investigation of electronically excited states of various small- and medium-sized organic molecules.[49−76] Send, Kaila, and Sundholm have shown that the reduction of the virtual-molecular-orbital space allows one to obtain relatively accurate CC2 excitation energies of large molecules at reduced computational effort.[71,77] Helmich and Hättig have shown that the introduction of pair-natural orbitals (PNOs) reduces the scaling of the resulting PNO-CC2 variant to $N^4$ and thus offers a significant speed-up for the calculation of CC2 excitation energies of large molecules.[78] Recent work by Martínez and co-workers has brought forth a tensor-hypercontracted (THC) variant of equation-of-motion (EOM-) CC2, which also reduces the scaling of the method to $N^4$.[79,80] Ledermüller and Schütz have presented analytical gradients for a CC2 method based on localized molecular orbitals.[81] Sneskov and Christiansen have provided a comprehensive review on coupled-cluster methods for the computation of electronically excited states.[57]

The algebraic-diagrammatic-construction (ADC) scheme of the polarization propagator was originally proposed by Schirmer.[82,83] Although the theoretical foundation of ADC has been available for more than three decades, implementations of ADC methods into the quantum-chemistry packages Turbomole,[39] Q-Chem,[84,85] and Psi4[46] have only recently begun to raise awareness of this method. The ADC formalism of the polarization propagator is based on many-body Green's function theory. The polarization propagator describes the effect of an external perturbation, such as the absorption of a photon, on the polarization of the electronic structure of a many-electron system. The ADC scheme offers an approximate and efficient method for the evaluation of the polarization propagator by means of Møller−Plesset perturbation theory and, as such, allows for the computation of excitation energies and transition moments of a molecular system. For the computation of electronically excited states, three main variants of ADC are in use today: the strict version of second-order ADC, ADC(2)-s, the extended version of second-order ADC, ADC(2)-x, and third-order ADC, ADC(3). The two variants of ADC(2) differ in the order at which the two-particle-two-hole block in the ADC matrix (that is, double excitations) is treated, that is, at zeroth order in the ADC(2)-s variant and at first order in the ADC(2)-x variant. The ADC(2)-x variant thus gives a qualitatively correct description of doubly excited states, although excitation energies are generally too low.[83,86,87] ADC(3), which is computationally only slightly more demanding than ADC(2)-x, remedies these problems and additionally offers significantly higher accuracy.[88] The ADC(2)-s method scales with $N^5$ (as does CC2), whereas the ADC(2)-x and ADC(3) methods both scale with $N^6$ (with slightly different prefactors).[82,83,86−88] Helmich and Hättig have presented PNO-ADC(2)-x, a variant that is based on pair-natural orbitals with a reduced scaling of $N^4$, as well as two alternative approaches for the perturbative correction for double excitations to the ADC(2)-s scheme, which shows improved accuracy over that of ADC(2)-x (which is inherently inaccurate due to missing second-order coupling elements for single and double excitations) for the computation of singlet excited states of double-excitation character.[89] Schütz has presented a local ADC(2) scheme and demonstrated its efficiency by optimizing several excited-state minima of a chlorophyll molecule.[90] Most recently, Lefrancois, Wormit, and Dreuw have presented a spin-flip variant of ADC and demonstrated its application to typical problems of strong multireference character in the electronic ground state.[91]

An advantage of the ADC methods over approximate CC methods is their Hermiticity, which avoids the breakdown in close vicinity of surface crossings, a well-known problem for CC methods.[42] ADC(3), in particular, scales with $N^6$, in contrast to $N^7$ for CC3, which allows the efficient calculation of significantly larger molecular systems at high accuracy. While CC methods describe the ground and excited states on an equal footing, the ADC methods describe the electronic ground state at the Møller−Plesset (MP) level at the respective order of perturbation theory, that is, MP2 in the case of ADC(2)-s and


DOI: 10.1021/acs.jctc.5b00022
J. Chem. Theory Comput. 2015, 11, 5758−5781

ADC(2)-x, and MP3 in the case of ADC(3).[86,87] However, CC2 ground-state energies and optimized geometries are not systematically superior to the ones obtained with MP2,[42] and in some cases, CC2 fails altogether.[92] On a related note, the MP2 ground-state energy is connected to the CC2 ground-state energy by means of neglecting specific amplitudes of the coupled-cluster equations. In this sense, MP2 is a simplification of ground-state CC2.[38] Finally, a close relationship between CC2 and ADC(2) has also been demonstrated by Hättig: the CC2 and ADC(2) Jacobi matrices, whose eigenvalues provide the excitation energies in linear-response theory, are connected by simple relations. However, while the CC2 Jacobi matrix is non-Hermitian, the ADC(2) Jacobi matrix is Hermitian.[42]

In recent years, ADC(2) (or ADC(3)) has been applied for the elucidation of the electronically excited states of organic molecules, for example, for the exploration of excited-state potential-energy surfaces,[76,93−106] for the QM/MM description of DNA components in aqueous solution,[107−109] as well as for nonadiabatic molecular-dynamics simulations of isolated molecules[101,110−113] and clusters or dimers,[72,114−116] for the calculation of excitation energies or absorption spectra of large molecular systems,[75,90,117−122] for the calculation of XPS,[123] NEXAFS,[121,123] and XAS[124] spectra of organic molecules, for the calculation of photoionization[125] and photoelectron[126,127] spectra, and for the calculation of solvatochromic shifts of aromatic chromophores.[128]

Spin-scaling approaches were first proposed as efficient and more accurate variants of the MP2 method. This idea was first introduced by Grimme in 2003, who partitioned the correlation energy into parallel and antiparallel spin components and scaled the weights of these two contributions by introducing two semiempirical parameters (scaling factors). This method was dubbed the spin-component-scaled (SCS) variant of MP2.[129] One year later, Head-Gordon and co-workers proposed to neglect the parallel-spin component altogether and instead increase the scaling factor for the antiparallel-spin contribution slightly. This method was dubbed the scaled-opposite-spin (SOS) variant of MP2.[130] In 2008, Hellweg, Grün, and Hättig implemented SCS and SOS variants of CC2 into Turbomole,[131] and Hättig and co-workers recently demonstrated the higher accuracy of SCS-CC2 against conventional CC2 for the calculation of 0−0 band origins of medium-sized and large organic molecules.[58] Krauter, Pernpointner, and Dreuw implemented an SOS variant of ADC(2)-s and ADC(2)-x into Q-Chem and demonstrated its applicability to larger molecules as well as its accuracy.[132] Grimme, Goerigk, and Fink have published an extensive review on spin-scaling approaches for various *ab initio* methods.[133]

A conical intersection is a point in molecular-coordinate space where two Born−Oppenheimer potential-energy surfaces of like multiplicity are isoenergetic and therefore intersect. The vicinity of a conical intersection is characterized by strong vibronic coupling, which leads to the breakdown of the Born−Oppenheimer approximation. The degeneracy at a point of conical intersection is lifted linearly at first order when displacing the molecular geometry along two specific nuclear-displacement vectors. These two degrees of freedom define the branching-plane or branching-space vectors (cf. Figure 2). The first vector is known as the gradient-difference vector **g**, which points in the direction of maximal energetic splitting. The second vector is known as the nonadiabatic-coupling vector **h**, which points in the direction of strongest nonadiabatic interaction of the two adiabatic electronic states. Displacement of the molecular geometry at a conical intersection along any of the remaining $3N - 8$ degrees of freedom retains the electronic degeneracy and merely moves the system along the $(3N - 8)$-dimensional seam of intersections between the two potential-energy surfaces (also called the intersection space). The intersection seam connects an infinite number of conical-intersection points and exhibits a topography that can be characterized by minima and transition states. Efficient algorithms for the geometry optimization of minimum-energy conical intersections are available in a number of quantum-chemistry programs these days. Aside from the minimum of the intersection seam, a number of methods has been developed for exploring the intersection seam.[5,134−137] Conical intersections are of comparable significance for nonadiabatic processes and nonluminescent photochemical reactions as are transition states for ground-state chemical reactions.[138−145] Therefore, the computational investigation of photochemical processes calls for electronic-structure methods that are able to correctly describe the potential-energy surfaces of two intersecting states in the vicinity of a conical intersection. This study aims at elucidating the performance of CC2 and ADC methods in the vicinity of the $S_1/S_0$ conical intersection driving the photoisomerization of PSB3.

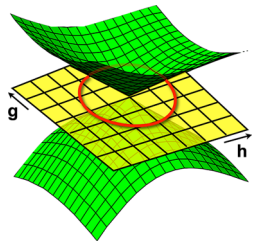


**Figure 2.** Graphical representation of two potential-energy surfaces intersecting at a conical intersection. The yellow plane depicts the branching plane, which is spanned by the two branching-plane vectors, the gradient-difference vector **g**, and the nonadiabatic-coupling vector **h**. The red circle represents a circular path around the conical intersection, which will be discussed later in the text.

The description of the topology, that is, the dimensionality of the branching space, of a conical intersection by a quantum-chemical method is another focus of this work. As we have shown in a previous study,[32] variational multiconfigurational wave-function methods, such as CASSCF, yield a correct description of the branching space and indeed yield a "conical" intersection. Other methods, such as certain multiconfigurational perturbative methods like SS-CASPT2 (but not MS-CASPT2), yield an incorrect description of the branching space and give a linear, as opposed to a conical, intersection, where the intersection seam is only $(3N - 7)$-dimensional. *From hereon, we refer to the latter cases as surface crossings to distinguish these from true conical intersections.* In general, methods that treat the two intersecting electronic states on an equal footing and include interstate-coupling elements in the Hamiltonian can be expected to yield a true conical intersection. Such methods are the CASSCF method, the MRCISD method, the multistate version of CASPT2 (MS-CASPT2), the XMCQDPT2 method,[32] and the SI-SA-REKS method.[30,13] On the other hand, methods that describe the intersecting states differently or do not include nonadiabatic coupling-matrix elements are expected to yield a linear crossing because the nonadiabatic-coupling vector is nonexistent for a method that cannot describe the vibronic coupling between the states. This has been shown for the single-state version of CASPT2 (SS-CASPT2), which treats each state by its own


DOI: 10.1021/acs.jctc.5b00022
J. Chem. Theory Comput. 2015, 11, 5758−5781

unperturbed and completely uncoupled Hamiltonian ($H_0$),[32] and for linear-response TDDFT.[32,146] A more detailed introduction to these issues can be found in ref 32.

For the CC2 method, it has already been demonstrated by comprehensive theoretical derivation by Hättig and by Köhn and Tajti that *the topology of surface crossings between excited states is incorrectly described*. This behavior is rooted in the non-Hermitian formulation of linear-response CC2.[42,147] Here, however, we consider only an $S_1/S_0$ surface crossing, which is different from the already studied case of excited-state surface crossings in the sense that the two intersecting states are not both response states and as such derived as eigenvalues of a non-Hermitian Jacobi matrix. Instead, only the $S_1$ excited state (the first response state) is derived from the Jacobi matrix, whereas *the ground state is the reference state for the CC2 linear-response formalism*. It is, therefore, thus far unclear how CC2 behaves at an $S_1/S_0$ surface crossing, since it has been deemed to be impossible to describe the strong multireference situation in the electronic ground state, which is found at an $S_1/S_0$ surface crossing, with a single-reference linear-response formalism, such as the CC2 method. For these reasons, an analysis of the behavior of the linear-response CC2 method for $S_1/S_0$ surface crossings, in other words, a surface crossing between the reference state and the first response state, is not available to date. For the ADC methods, on the other hand, the electronic ground state is described at a different level of theory, that is, the MP2 or MP3 level. This means that due to the description of the intersecting states at different levels of theory (which naturally excludes any coupling between the states), an $S_1/S_0$ surface crossing cannot be expected to present as a true conical intersection but as a linear intersection instead.

In this article, we report on a comprehensive evaluation of the performance of CC2 and ADC methods for the description of $S_0$ and $S_1$ reaction paths as well as of the branching space of the conical intersection involved in the photoisomerization process of PSB3. To that end, we combine the most relevant pathways and explorations of the immediate vicinity of the conical intersection from our previous benchmark studies, that is, the ground-state bond-length-alternation (BLA) pathway, the diradicaloid minimum-energy path ($MEP_{DIR}$), the charge-transfer minimum-energy path ($MEP_{CT}$), the excited-state minimum-energy path from the *cis* isomer to the conical-intersection seam ($MEP_{cis}$), the excited-state minimum-energy path from the *trans* isomer to the conical-intersection seam ($MEP_{trans}$), a scan along the conical-intersection seam, and, finally, a scan along a circular path centered at the conical intersection as well as a two-dimensional scan of the two intersecting potential-energy surfaces along the branching space.[27,31,32] Apart from these previously introduced pathways, we present a new evaluation of the CC2 and ADC(2)-s gradient-difference vectors along a circular path around the surface crossing. Details on these pathways are given in the Methods section. We also evaluate the performance of a penalty-function algorithm developed by Levine, Coe, and Martínez[148] for the approximate optimization of the minimum-energy conical intersection of PSB3 with the CC2 and the ADC(2)-s methods. In total, the methods tested herein comprise CC2, SOS-CC2, ADC(2)-s, SOS-ADC(2)-s, ADC(2)-x, SOS-ADC(2)-x, and ADC(3), with additional evaluations of selected SCS variants given in the Supporting Information. The performance of these methods will be evaluated with respect to the reference energy profiles computed at the CASSCF and MRCISD+Q levels, as previously presented in the earlier contributions of this series.

## 2. METHODS

**2.1. Preface on the ADC Methods.** Since ADC methods are linear-response methods that yield excitation energies directly from the polarization-propagator formalism, an ADC level of theory for the electronic ground state does not exist. Following the derivation of ADC approaches via the intermediate-state-representation (ISR) formalism,[149] the ADC(2) matrix representing the shifted Hamiltonian as well as the intermediate-state basis is constructed with respect to the MP2 ground-state energy and wave function, respectively. The same holds for the higher-order ADC($n$) schemes and their relation to the corresponding MP$n$ ground state. Accordingly, the corresponding MP ground-state energy is the most natural choice for the calculation of total energies, and a corresponding expression for the total energy of an excited state within the ISR-derived ADC schemes has already been provided in ref 149. For this reason, in studies employing ADC methods, the electronic ground state is usually described by the MP2 (in the case of ADC(2)-s and ADC(2)-x) or MP3 (in the case of ADC(3)) method. Total energies of excited states are given as the sum of the underlying MP ground-state total energy and the ADC excitation energy derived from linear-response theory. We adopt the following *convention for the figures presented in this work:* for the potential-energy profiles computed with an ADC method, the ground-state curve or surface is labeled as MP, whereas the excited-state curve or surface is labeled as ADC.

**2.2. *Ab Initio* Methods and Quantum-Chemistry Codes.** The Turbomole 6.6 program package[39,150] was used for the calculations employing the approximate coupled-cluster method of second order (CC2), the spin-component-scaled variant of the CC2 method (SCS-CC2), and the scaled-opposite-spin variant of CC2 (SOS-CC2).[150] For the two spin-scaled CC2 methods, the default scaling factors of $c_{ss} = {}^1/_3$ and $c_{os} = {}^6/_5$ for SCS-CC2 and $c_{ss} = 0$ and $c_{os} = 1.3$ for SOS-CC2 were used. Throughout all calculations, the basis set 6-31G* with Cartesian d functions was used as well as the resolution-of-the-identity (RI) approximation,[40] the latter of which requires the use of an auxiliary-basis set. Since Turbomole does not provide an optimized auxiliary-basis set for RI calculations with the basis set 6-31G*, we used the auxiliary-basis set for the basis set def2-SV(P) instead (the basis sets 6-31G* and def2-SV(P) exhibit very similar contraction schemes). Also, the frozen-core approximation was used, in which the 1s orbitals of the first-row atoms are frozen at the Hartree−Fock level. The results obtained along selected pathways using the SCS variants of CC2 and ADC(2)-s available in Turbomole are shown in Figures S28−S34 in the Supporting Information.

The Q-Chem 4.2 program package[85] was used for the calculations employing the algebraic-diagrammatic-construction (ADC) scheme for the polarization propagator of second order in the strict and extended variants, that is, ADC(2)-s and ADC(2)-x,[87] as well as the SOS variants of these two methods, SOS-ADC(2)-s and SOS-ADC(2)-x.[132] For SOS-ADC(2)-s, the scaling parameters $c_{os} = 1.3$ and $c_{os}^{coupling} = 1.17$ were used, whereas for SOS-ADC(2)-x, the parameters $c_{os} = 1.3$, $c_{os}^{coupling} = 1.0$, and $c_x = 0.9$ were used. For the calculations at the third-order ADC(3) level,[88,151] a developers' version of the `adcman` module within the Q-Chem 4.21 package was used.[86] Again, the 6-31G* basis set was used throughout all calculations. The RI approximation was not used.

For ADC methods, the reference state, that is, the electronic ground state, is treated at the respective order of Møller−Plesset


DOI: 10.1021/acs.jctc.5b00022
J. Chem. Theory Comput. 2015, 11, 5758−5781

perturbation theory. Thus, the energy profiles of the reference state for the ADC(2)-s and ADC(2)-x methods correspond to the MP2 level of theory, whereas for SOS-ADC(2)-s and SOS-ADC(2)-x, they correspond to the SOS-MP2 level. Finally, for ADC(3), the reference state is treated at the MP3 level.

The CASSCF branching-space vectors were obtained by optimizing the twisted $S_1/S_0$ minimum-energy conical intersection of PSB3 in Gaussian 03[152] including the full $\pi$-electron system in the active space and equally averaging over the two lowest roots with the basis set 6-31G* (SA2-CASSCF(6,6)/6-31G*). The MRCISD branching-space vectors were obtained by optimizing the $S_1/S_0$ minimum-energy conical intersection of PSB3 analogously to the description in the paper by Nikiforov et al.,[15] albeit using a full-$\pi$ active space of (6,6) and the basis set 6-31G* for consistency with this series of papers. This calculation was performed in Columbus 7.[153] The CASSCF and MRCISD branching-space vectors were orthogonalized via the Yarkony procedure[154] and normalized before they were used for the construction of the circles and 2D scans around the conical intersection. A comparison of the CASSCF- and the MRCISD-optimized minimum-energy conical intersection as well as the orthonormalized CASSCF and MRCISD branching-space vectors is shown in Figure S1 in the Supporting Information. The gradient-difference vectors for the CC2 and the ADC(2)-s methods were evaluated by subtraction of the gradient of the reference state from the gradient of the response state, which were obtained in Turbomole.

Throughout all figures, the energies are given in kcal/mol relative to the energy of *trans*-PSB3, which is the more stable isomer of PSB3.

**2.3. Reference Reaction Paths.** We use the ground- and excited-state pathways introduced in earlier contributions of this benchmark series,[27,31,32] the structures of which were optimized or constructed at the SA2-CASSCF(6,6)/6-31G* level. The BLA pathway scans the bond-length-alternation coordinate (cf. Figure 3a) and connects the transition state for the charge-transfer isomerization path ($TS_{CT}$), the $S_1/S_0$ conical intersection driving the photoisomerization process, and the transition state for the diradicaloid isomerization path ($TS_{DIR}$) (cf. Figure 3b). The charge-transfer minimum-energy path ($MEP_{CT}$) connects *cis*-PSB3, $TS_{CT}$, and *trans*-PSB3 (and is centered in the region near $TS_{CT}$), whereas the diradicaloid minimum-energy path ($MEP_{DIR}$) connects *cis*-PSB3, $TS_{DIR}$, and *trans*-PSB3 (and is centered in the region near $TS_{DIR}$, cf. Figure 3b). These two pathways involve the hydrogen out-of-plane (HOOP) motion (cf. Figure 3a). The composite pathway in the $S_1$ excited state is composed of three pathways (cf. Figure 3c): the *cis*-side minimum-energy path ($MEP_{cis}$), which connects *cis*-PSB3 with a *cisoid* conical intersection; the conical-intersection-seam pathway, which involves the HOOP motion and connects the *cisoid* conical intersection ($CI_{cis}$), the conical intersection ($CI_{BLA}$), and the *transoid* conical intersection ($CI_{trans}$); and the *trans*-side minimum-energy path ($MEP_{trans}$), which connects *trans*-PSB3 with the *transoid* conical intersection ($CI_{trans}$). Apart from these pathways, we also test each method along a circle centered at a selected point on the conical-intersection seam (cf. Figure 2), which was determined by the $S_1/S_0$ crossing point along the BLA scan separately for each method, except for the CASSCF and MRCISD methods, for which we used the optimized minimum-energy conical intersections instead. Around this geometry, a circle with a radius of 0.02 Å was constructed for each method in increments of 10° *by using the orthonormalized branching-plane vectors determined at the CASSCF level.* (For the MRCISD+Q method, we used a radius of 0.01 Å because a radius of 0.02 Å resulted in a number of artifacts. For the CC2 method, we used a radius of 0.03 Å because a radius of 0.02 Å resulted in a discontinuous energy profile due to unconverged points. Furthermore, we used a finer increment of 1° for the CC2 method.) For comparison, we also constructed the circles for the CASSCF method using a smaller radius of 0.002 Å as well as using MRCISD branching-plane vectors, which is shown in Figure S18 in the Supporting Information. For the construction of the 2D-surface plots in the branching plane, the same crossing points and orthonormalized branching-plane vectors were used. These scans were constructed by displacing the geometry of the crossing point by up to 0.05 Å in each direction. For the CC2 method, a roughly three times finer grid was used than for the other methods. For comparison, we also constructed these 2D scans for select methods using the orthonormalized branching-plane vectors computed at the MRCISD level of theory (cf. Figure S18 in the Supporting Information). The reader interested in the technical details on the construction of the various pathways is referred to the original papers.[27,31,32]

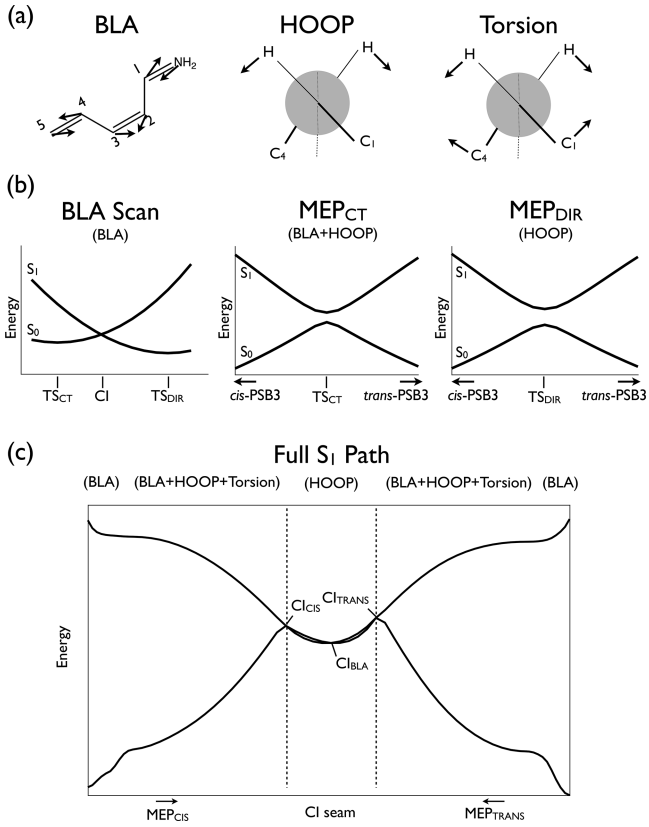


**Figure 3.** Schematic representations of relevant intramolecular coordinates and reaction paths. (a) The bond-length alternation (BLA) mode, the hydrogen out-of-plane (HOOP) mode, and the torsion mode; (b) $S_0$ and $S_1$ CASSCF energy profiles along the BLA, $MEP_{CT}$, and $MEP_{DIR}$ pathways as well as stationary points involved in these pathways given on the *x*-axis. The BLA path intersects $TS_{CT}$, the conical intersection (CI), and $TS_{DIR}$; the $MEP_{CT}$ path connects $TS_{CT}$ with *cis*- and *trans*-PSB3; the $MEP_{DIR}$ path connects $TS_{DIR}$ with *cis*- and *trans*-PSB3. (c) $S_0$ and $S_1$ CASSCF energy profiles along the composite $S_1$ path connecting the $MEP_{cis}$ pathway, the $CI_{cis}$−$CI_{BLA}$−$CI_{trans}$ seam (CI seam), and the $MEP_{trans}$ pathway.

**2.4. Charge-Transfer Character.** In its ground-state *cis* or *trans* equilibrium geometry, PSB3 is a cation with the positive



DOI: 10.1021/acs.jctc.5b00022
J. Chem. Theory Comput. 2015, 11, 5758−5781

charge localized mainly on the Schiff-base nitrogen atom (on the iminium fragment). When PSB3 develops charge-transfer character, the positive charge translocates partially or fully across the central double bond to the other side of the molecule (on the allyl fragment). To quantify the charge transfer, we compute the charge-transfer character by summing the Mulliken charges of all the atoms of the allyl fragment ($H_2C5{=}C4H{-}C3H{=}$; cf. Figure 1 for the numbering of atoms). Since the computation of Mulliken charges at the MP2 and MP3 levels is not yet implemented in Q-Chem, we show the charge-transfer character only for those methods for which Mulliken charges are available in Turbomole, that is, the CC2 and SOS-CC2 methods as well as the ADC(2)-s and SOS-ADC(2)-s methods (since we consider only the charge-transfer character of the reference state, the Mulliken charges computed for the latter two methods correspond to the Mulliken charges at the MP2 and SOS-MP2 levels, respectively). Since Mulliken charges cannot be computed at the MRCISD+Q level, the charge-transfer character was determined at the MRCISD level instead.

**2.5. Nonparallelity Errors.** We evaluate nonparallelity errors (NPEs) of a given method as a measure for the deviation of the energy profile obtained with this method from the energy profile obtained with a reference method along a given pathway. We use the energy profiles obtained with the MRCISD+Q method for reference. NPEs are computed by subtracting the minimum-energy deviation from the maximum-energy deviation, where the energy deviations between a method and the reference method are evaluated at each point of a given pathway. A small NPE, therefore, corresponds to an energy profile that runs fairly parallel to the energy profile of the reference method, whereas a large NPE hints at a deviation in the shape of the potential-energy surface and thus to a large extent of nonparallelity in the energy profiles along a given pathway obtained with two different methods.

**2.6. Approximate Geometry Optimization of Minimum-Energy Conical Intersections at the CC2 and ADC(2)-s/MP2 Levels.** For the approximate optimization of the minimum-energy conical intersection driving the photoisomerization of the central double bond of PSB3, we used the program CIOpt developed by Levine, Coe, and Martínez.[148] The underlying algorithm employing a penalty function allows the approximate optimization of a minimum-energy conical intersection for any electronic-structure method capable of determining the energy of electronically excited states. The program CIOpt was interfaced with Turbomole to optimize the minimum-energy conical intersection of PSB3 at the CC2 as well as at the mixed ADC(2)-s/MP2 level of theory. The same settings regarding the basis set and the auxiliary basis set were used as specified above. Note that from all of the ADC variants tested in this work only the ADC(2)-s variant is implemented in Turbomole.

## 3. RESULTS

**3.1. BLA Path.** The energy profiles along the bond-length-alternation (BLA) scan are shown in Figure 4. The BLA scan intersects, in that order, $TS_{CT}$, $CI_{BLA}$, and $TS_{DIR}$, whose positions are shown by vertical dashed lines. As already pointed out in a previous paper of this series, the CASSCF method overestimates the energy of the two transition states, $TS_{CT}$ and $TS_{DIR}$, and gives an incorrect energy order by predicting $TS_{DIR}$ to be more stable than $TS_{CT}$. These shortcomings can be attributed to the lack of dynamical correlation in the CASSCF method. Upon inclusion of dynamical correlation using the MRCISD+Q reference

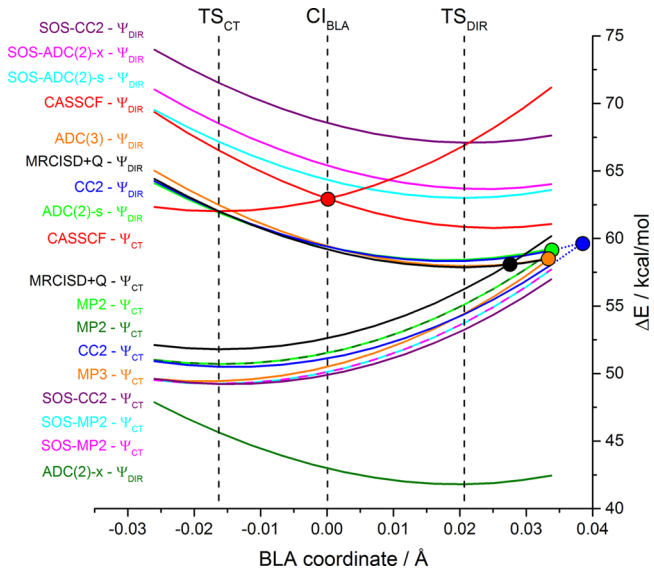


**Figure 4.** Energy profiles (in kcal/mol relative to *trans*-PSB3) of CC2 and ADC methods including SOS variants along the BLA coordinate of PSB3. The curves are labeled at the left to distinguish diabatic potential-energy curves of mainly charge-transfer character ($\Psi_{CT}$) and covalent-diradical character ($\Psi_{DIR}$). $S_0$ and $S_1$ energies are given for the CC2 (blue), SOS-CC2 (purple), ADC(2)-s (green), SOS-ADC(2)-s (cyan), ADC(2)-x (olive), SOS-ADC(2)-x (magenta), and ADC(3) (orange) methods as well as for the CASSCF (red) and MRCISD+Q (black) methods for reference. $S_0$ energies obtained for the ADC(2)-s and ADC(2)-x, as well as for the SOS-ADC(2)-s and SOS-ADC(2)-x methods, respectively, are equal (i.e., they correspond to the MP2 and SOS-MP2 levels, respectively) and are given as dashed lines. The positions of the transition states $TS_{CT}$ and $TS_{DIR}$ as well as the conical intersection intercepted by the BLA scan, $CI_{BLA}$, are indicated by the vertical dashed lines in black. The approximate position of the surface crossings for the other methods is indicated by a filled circle. The surface crossing for the CC2 method is located slightly outside the original BLA pathway and was located by extrapolation of the original pathway (dotted blue lines). The surface crossings for the remaining methods are located further outside the original BLA pathway (on the extrapolated pathway) and are not shown.

method, the peaked CASSCF conical intersection $CI_{BLA}$ located in the middle of the BLA pathway moves toward $TS_{DIR}$ and changes its topography toward a sloped conical intersection, as shown by the curve for the MRCISD+Q method. Also, the energy order of $TS_{CT}$ and $TS_{DIR}$ is reversed. These effects have been rationalized in detail in a previous contribution of this benchmark series.[27]

Comparing the energy of the $\Psi_{CT}$ curves of the CC2 and ADC methods with the MRCISD+Q reference values reveals that all CC2 and ADC methods tend to slightly overstabilize the charge-transfer state, $\Psi_{CT}$, but otherwise run fairly parallel to the MRCISD+Q curve. The effect of overstabilization of $\Psi_{CT}$ is smallest for ADC(2)-s and ADC(2)-x and slightly larger for ADC(3), SOS-ADC(2)-s, and SOS-ADC(2)-x.

In the case of the diradical state, $\Psi_{DIR}$, we see a higher degree of variability in the energy among the different CC2 and ADC variants. $\Psi_{DIR}$ exhibits open-shell character and, hence, a significant multiconfigurational character. The dramatic overstabilization of $\Psi_{DIR}$ by the ADC(2)-x method and, most importantly, the fact that the ADC(2)-x method reverses the energy order of $\Psi_{DIR}$ and $\Psi_{CT}$ shows that $\Psi_{DIR}$ also exhibits significant double-excitation character, in contrast to $\Psi_{CT}$. The ADC(2)-x method overcompensates this effect and, hence,


DOI: 10.1021/acs.jctc.5b00022
J. Chem. Theory Comput. 2015, 11, 5758−5781

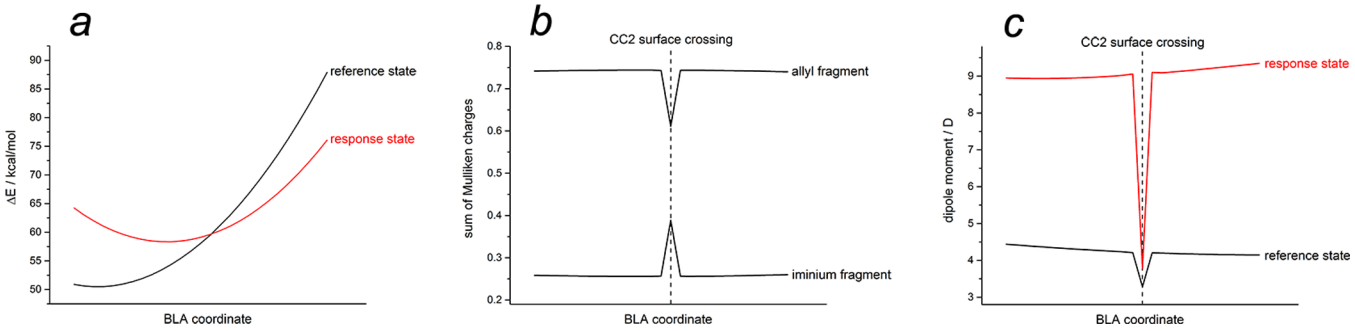


**Figure 5.** Behavior of the linear-response CC2 method along the BLA coordinate extended beyond the surface crossing by extrapolation of the original BLA pathway. (a) Energy profiles of the reference (black) and response (red) states. (b) Sum of Mulliken charges of the reference state for the allyl and the iminium fragment of PSB3. (c) Dipole moments (in D) of the reference (black) and response (red) states.

underestimates excitation energies of excited states of double-excitation character, in contrast to excited states of single-excitation character. This is due to the, with respect to the singly excited configurations, unbalanced inclusion of doubly excited configurations at only the first order of perturbation theory in the formulation of the ADC(2)-x method (the singly excited configurations are included at second order).[86,87] Nonetheless, $\Psi_{DIR}$ is well-described by CC2, ADC(2)-s, and ADC(3), whose energy profiles run fairly parallel and close to the MRCISD+Q values. On the other hand, it is obvious that the SOS variants of all tested methods, SOS-CC2, SOS-ADC(2)-s, and SOS-ADC(2)-x, dramatically overestimate the energy of $\Psi_{DIR}$, which is likely due to the failure of SOS methods to correctly describe a response state of multiconfigurational character.

The relative energies of $\Psi_{DIR}$ and $\Psi_{CT}$ determine the geometry, energy, and even the topography of the surface crossing $CI_{BLA}$. As discussed in earlier work,[27] the MRCISD+Q surface crossing has a higher BLA value than that of the CASSCF crossing. It exhibits a sloped-intermediate topography, in contrast to the peaked topography of the CASSCF crossing. We find that the CC2 surface crossing has an even higher BLA value than that of the MRCISD+Q crossing, since CC2 slightly overstabilizes $\Psi_{CT}$. In fact, the CC2 crossing lies slightly outside the original BLA path and was found by extrapolation of the original BLA pathway, that is, by generating new structures using the nuclear displacements of the BLA coordinate. This is similar to the results obtained at the EOM-CCSD level in an earlier benchmark study.[28] The ADC(2)-s and ADC(3) surface crossings lie closer to that of MRCISD+Q and, thus, these methods perform better in this case than CC2. The other methods, on the other hand, show surface crossings that are significantly displaced with respect to the MRCISD+Q crossing, to such an extent that they do not appear in the range shown in Figure 4. In fact, SOS-ADC(2)-x, SOS-ADC(2)-s, and SOS-CC2 show surface crossings at large BLA values (obtained by extrapolation of the original path) due to their destabilizing $\Psi_{DIR}$ (these surface crossings have BLA values of 0.055, 0.055, and 0.07 Å, respectively). Quite differently, the surface crossing of ADC(2)-x is found at a negative BLA value (−0.04 Å) due to its dramatic overstabilization of $\Psi_{DIR}$.

The behavior of the CC2 method beyond the surface crossing, that is, for high BLA values obtained by extrapolation of the original BLA pathway, is shown in Figure 5. Beyond the surface crossing, the reference state, that is, the state which is computed as the electronic ground state, remains on the $\Psi_{CT}$ curve, whereas the response state, that is, the excited state, remains on the $\Psi_{DIR}$ curve (cf. Figure 5a). This leads to the peculiar observation of negative excitation energies, which one obtains beyond the surface crossing. This is analogous to what has been described by Martínez and co-workers for linear-response TDDFT.[146] However, even though the surface crossing presents a case of strong ground-state multireference character, the CC2 method converges and does not exhibit any artifacts in this instance. The only discontinuities that we could identify are the Mulliken charges of the allyl and iminium fragments in the reference state, where we see a spike at the location of the surface crossing (cf. Figure 5b) and in the dipole moments of the two states, which also exhibit a spike (cf. Figure 5c). We could not identify any obvious cause for the occurrence of these spikes.

**3.2. $MEP_{CT}$ Path.** The energy profiles and the charge-transfer character along the $MEP_{CT}$ path are shown in Figure 6a,b. As shown in part a, the CASSCF method overestimates the energy barrier at $TS_{CT}$, which is corrected by inclusion of dynamical electron correlation, as shown for the MRCISD+Q method. All CC2 and MP methods underestimate the energy barrier with respect to the MRCISD+Q reference values. SOS-CC2 and SOS-MP2 give the lowest barrier heights at $TS_{CT}$. Remarkably, the MP2 method comes closest to the reference value at the MRCISD+Q level. Away from the transition state, SOS-CC2 and CC2 underestimate the energy slightly, whereas SOS-MP2, MP2, and MP3 overestimate it. The $S_1$ energy profiles along the $MEP_{CT}$ scan are shown in Figure S2 in the Supporting Information.

The profiles of the charge-transfer character shown in Figure 6b show that the CC2 method reproduces the behavior of the MRCISD curve qualitatively best, although the charge-transfer character is slightly too low. Those methods that have been shown to overstabilize $\Psi_{CT}$ with respect to the MRCISD+Q reference values in the BLA scan shown in Figure 4 exhibit a broader charge-transfer region than that observed for the MRCISD values shown in Figure 6b. The SOS-CC2 method smears out the peak of the charge-transfer character over a larger region and falls off too slowly. The SOS-MP2 and MP2 methods deviate strongly from the MRCISD values: the region of strong charge-transfer character is too broad and falls off too slowly with increasing distance from the transition state. Exemplary for the linear-response methods, the decrease in the charge-transfer character of the CC2 reference state can be understood by recognizing the change in the molecular $\pi$ orbitals along the $MEP_{CT}$ path. At $TS_{CT}$, the HOMO and LUMO are fully localized on the iminium and allyl moieties, respectively. The same applies to the remainder of the $\pi$ orbitals. This localization of the $\pi$ orbitals results in a strong charge-transfer character. When the geometry of $TS_{CT}$ is displaced along the isomerization


DOI: 10.1021/acs.jctc.5b00022
J. Chem. Theory Comput. 2015, 11, 5758−5781

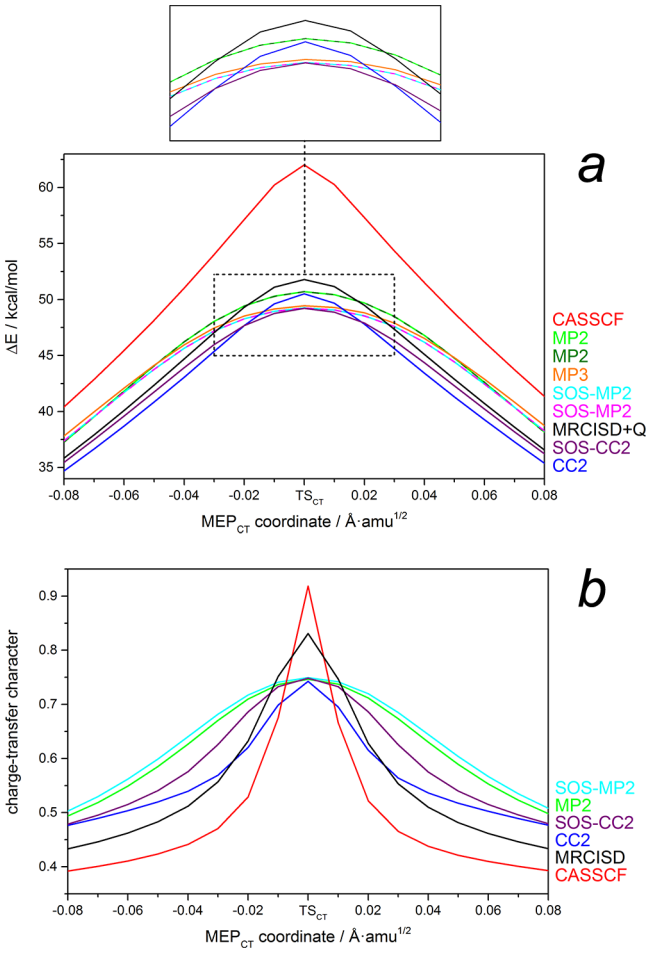


**Figure 6.** (a) $S_0$ energy profiles (in kcal/mol) along the $MEP_{CT}$ pathway, which connects $TS_{CT}$ (in the middle of the plot) with *cis*- and *trans*-PSB3 (which lie outside the plotted region, at values of −0.54 and 0.65 Å·amu$^{1/2}$, respectively). $S_0$ energies are given for the CC2 (blue), SOS-CC2 (purple), MP2 (green and olive), SOS-MP2 (cyan and magenta), and MP3 (orange) methods as well as for the CASSCF (red) and MRCISD+Q (black) reference methods. (b) Charge-transfer character along the $MEP_{CT}$ pathway for the CC2, SOS-CC2, MP2, SOS-MP2, CASSCF, and MRCISD methods.

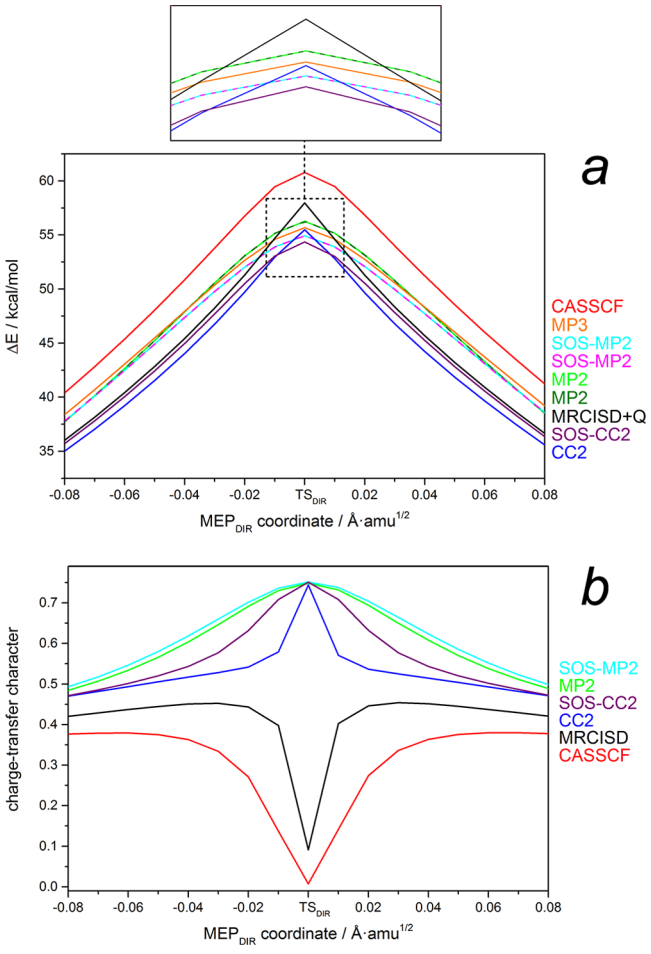


**Figure 7.** (a) $S_0$ energy profiles (in kcal/mol) along the $MEP_{DIR}$ pathway, which connects $TS_{DIR}$ (in the middle of the plot) with *cis*- and *trans*-PSB3 (which lie outside the plotted region, at values of −0.52 and 0.66 Å·amu$^{1/2}$, respectively). The $S_0$ energies are given for the CC2 (blue), SOS-CC2 (purple), MP2 (green and olive), SOS-MP2 (cyan and magenta), and MP3 (orange) methods as well as for the CASSCF (red) and MRCISD+Q (black) reference methods. (b) Charge-transfer character along the $MEP_{DIR}$ pathway for the CC2, SOS-CC2, MP2, SOS-MP2, CASSCF, and MRCISD methods.

coordinate, the $\pi$ orbitals develop an increasing level of delocalization over the entire molecule, which gradually reinstates the central double bond of PSB3 toward the planar ground-state minima. This delocalization of the $\pi$ orbitals results in decreasing charge-transfer character.

**3.3. $MEP_{DIR}$ Path.** The energy profiles and charge-transfer character along the $MEP_{DIR}$ path are shown in Figure 7a,b. For the energy profiles, the same trends are observed as for those along the $MEP_{CT}$ path. This is due to the fact that for all CC2 and ADC methods (with the exception of ADC(2)-x) the $\Psi_{CT}$ state is stabilized with respect to $\Psi_{DIR}$ (cf. Figure 4) and therefore causes the character of the ground-state wave function of $TS_{DIR}$ to change from diradical (at the CASSCF level of theory) to charge transfer. Therefore, the $MEP_{DIR}$ path, which was constructed at the CASSCF level of theory, passes through a region of charge-transfer character in the vicinity of the transition state $TS_{DIR}$, and the profiles along the $MEP_{DIR}$ path behave similarly to the ones along $MEP_{CT}$. This is also reflected in the profiles for the charge-transfer character presented in Figure 7b, where we find that CC2 and MP methods gain charge-transfer character, as opposed to CASSCF and MRCISD, both of which retain diradical character at $TS_{DIR}$.[27]

The charge-transfer character given in Figure 7b shows that the CC2 and MP2 methods as well as their SOS variants exhibit an inverted charge-transfer profile compared to those of CASSCF and MRCISD. This is due to the fact that the surface crossing is shifted so far along the BLA path that $TS_{DIR}$ is no longer located on the diradical state but, rather, on the charge-transfer state, which results in the strong charge-transfer character at the $TS_{DIR}$ geometry.

The $S_1$ energy profiles along the $MEP_{DIR}$ scan are shown in Figure S3 in the Supporting Information.

**3.4. Composite $S_1$ Path.** The $S_0$ and $S_1$ energy profiles along the composite $S_1$ path obtained with CASSCF-constructed geometries are shown in Figure 8. The features of the CASSCF potential-energy surfaces and the MRCISD+Q-corrected surfaces are discussed in detail in ref 31. Here, we note that dynamical electron correlation introduced by MRCISD+Q causes an excited-state minimum to develop in the vicinity of the Franck−Condon region near *cis*- and *trans*-PSB3. We optimized these minima at the CASPT2 level of theory as part


DOI: 10.1021/acs.jctc.5b00022
J. Chem. Theory Comput. 2015, 11, 5758−5781

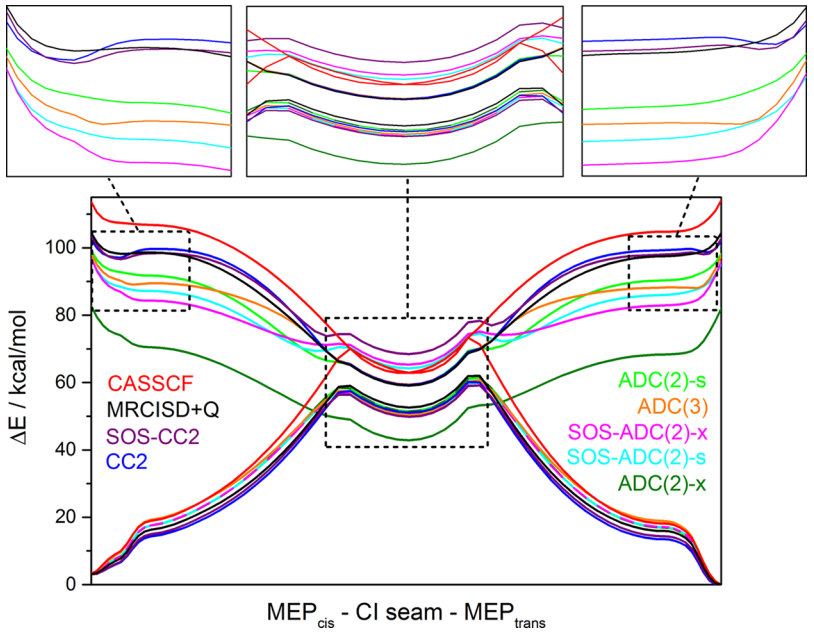


**Figure 8.** Energy profiles (in kcal/mol) along the composite CASSCF $S_1$ pathway, which is composed of the $MEP_{cis}$, the conical-intersection (CI) seam, and the $MEP_{trans}$ pathways. $S_0$ and $S_1$ energies are given for the CC2 (blue), SOS-CC2 (purple), ADC(2)-s (green), SOS-ADC(2)-s (cyan), ADC(2)-x (olive), SOS-ADC(2)-x (magenta), and ADC(3) (orange) methods as well as for the CASSCF (red) and MRCISD+Q (black) reference methods. $S_0$ energies obtained for the ADC(2)-s and ADC(2)-x methods, as well as for the SOS-ADC(2)-s and SOS-ADC(2)-x methods, respectively, are equal (i.e., they correspond to the MP2 and SOS-MP2 levels, respectively) and are given as dashed lines.

of a previous contribution.[31] We also find that the degeneracy at the CASSCF conical-intersection seam is split due to an unequal stabilization of $\Psi_{CT}$ and $\Psi_{DIR}$, yet the extent of splitting varies among the various methods (as already observed in Figure 4). Also, all methods yield a minimum on the conical-intersection seam, that is, the conical intersection $CI_{BLA}$, which is located in the center of the conical-intersection seam, is, as it should be, an actual minimum on the conical-intersection seam.

In Figure 8, we also notice a wide variability in the $S_1$ relative energies of the different CC2, ADC, and multiconfigurational methods, with ADC(2)-x giving the lowest excited-state energy with respect to the ground state and CASSCF giving the highest energy (due to the missing dynamical electron correlation). All ADC variants give lower excited-state energies than MRCISD+Q, whereas CC2 and SOS-CC2 give more similar energies to those of MRCISD+Q (although in the case of SOS-CC2 it deviates significantly at the conical-intersection seam). We also notice that the shape of the excited-state potential-energy surfaces near the Franck−Condon regions varies markedly for the different methods. For instance, CC2 and SOS-CC2 give a well-defined minimum close to the Franck−Condon regions of *cis*- and *trans*-PSB3, similar to MRCISD+Q. ADC(3) also displays a minimum, although a shallower one. However, ADC(2)-s, ADC(2)-x, SOS-ADC(2)-s, and SOS-ADC(2)-x show no minimum, similar to CASSCF.

Looking at the complete $S_1$ path, the energy profile of the CC2 method runs remarkably parallel to the MRCISD+Q energy profiles. The SOS-CC2 method runs parallel to the MRCISD+Q profile in the $MEP_{cis}$ and $MEP_{trans}$ parts of the scan, yet it deviates significantly in the $CI_{seam}$ part. All ADC methods deviate significantly from the entire $S_1$ energy profile of the MRCISD+Q method in the excited state, although the ADC(2)-s method seems to consistently underestimate the reference values, albeit running fairly parallel to them. For the $S_0$ state, on the other hand, all CC2 and MP methods agree well with the MRCISD+Q profile.

In an earlier study,[31] we also optimized the same composite $S_1$ path comprising $MEP_{cis}$, the conical-intersection seam, and $MEP_{trans}$ at the CASPT2 level of theory. For the sake of brevity, we do not discuss CC2 and ADC energy profiles along this path here. We refer the interested reader to Figure S4 in the Supporting Information as well as to ref 31.

Table 1 shows the nonparallelity errors (NPEs) of the energy profiles obtained with various methods along the $S_1$ composite path constructed of geometries obtained with the CASSCF method against the energy profile of the reference MRCISD+Q method. In detail, Table 1 provides the NPEs along the full $S_0$ path, along the full $S_1$ path, along the $S_0$ conical-intersection seam, and along the $S_1$ conical-intersection seam. Since MRCISD+Q is chosen as the reference method, the NPEs for this method vanish throughout all the pathways. The comparison

**Table 1. NPEs (in kcal/mol) for Various Methods along the Full $S_1$ CASSCF Path and along the Conical-Intersection Seam**

| method | composite path $S_0$ NPE | composite path $S_1$ NPE | CI seam $S_0$ NPE | CI seam $S_1$ NPE |
|---|---|---|---|---|
| MRCISD+Q | 0.0 | 0.0 | 0.0 | 0.0 |
| CASSCF | 11.4 | 6.0 | 1.6 | 1.2 |
| CC2 | 2.6 | 5.9 | 0.3 | 0.2 |
| SOS-CC2 | 3.0 | 11.2 | 0.2 | 0.2 |
| ADC(2)-s/MP2 | 3.8 | 7.9 | 0.4 | 0.5 |
| SOS-ADC(2)-s/SOS-MP2 | 4.8 | 16.8 | 0.4 | 0.2 |
| ADC(2)-x/MP2 | 3.8 | 13.1 | 0.4 | 0.1 |
| SOS-ADC(2)-x/SOS-MP2 | 4.8 | 20.9 | 0.4 | 0.5 |
| ADC(3)/MP3 | 5.5 | 10.8 | 0.5 | 0.1 |



DOI: 10.1021/acs.jctc.5b00022
J. Chem. Theory Comput. 2015, 11, 5758−5781

of the CC2 and SOS-CC2 values reveals that CC2 gives the smallest NPE for the full $S_0$ pathway among all tested methods (2.6 kcal/mol), whereas the NPE of the SOS-CC2 method is slightly larger (3.0 kcal/mol). For the full $S_1$ pathway, on the other hand, CC2 gives the lowest NPE, whereas SOS-CC2 gives a large NPE. The latter arises from the fact that SOS-CC2 runs close to the MRCISD+Q reference profile in the $MEP_{cis}$ and $MEP_{trans}$ parts of the composite pathway, but it is shifted about 9 kcal/mol in the conical-intersection-seam part, which is likely due to the failure of SOS methods to describe multiconfigurational response states. The consistent parallelity of the SOS-CC2 method within the conical-intersection seam is demonstrated by the small NPE of 0.2 kcal/mol within the conical-intersection seam, which is equal to the NPE of CC2. This means that although the SOS-CC2 method overestimates the MRCISD+Q reference values by 9 kcal/mol within the conical-intersection seam, it does so consistently and the profile is therefore fairly parallel to the MRCISD+Q profile. The ADC(2)-s/MP2 method shows only slightly larger NPEs for the full $S_0$ and $S_1$ paths than those for CC2 (3.8 and 7.9 kcal/mol), which reinforces the picture discussed above, where the ADC(2)-s $S_1$ curve is almost perfectly parallel to the MRCISD+Q curve. Both SOS-ADC(2) methods as well as ADC(2)-x and ADC(3) show a large NPE for the $S_1$ path. The ADC(2)-x method consistently underestimates the $S_1$ energy, but the level of overstabilization varies from the MEP paths to the conical-intersection seam, which results in the largest NPE for the full $S_1$ path (20.9 kcal/mol).

$S_0$−$S_1$ energy gaps for the various methods at five important geometries, that is, *cis*-PSB3, *trans*-PSB3, $CI_{cis}$, $CI_{BLA}$, and $CI_{trans}$, are given in Table S1 in the Supporting Information.

**3.5. Circular Path around the Surface Crossing.** The energy difference along the circles around the conical intersection or surface crossing constructed for the optimized conical intersections (in the case of CASSCF and MRCISD) or approximate surface crossings (in the case of the linear-response methods) using the orthonormalized branching-plane vectors (which were determined at the CASSCF level) is shown in Figure 9. The CASSCF method shows the physically correct behavior for a true conical intersection: the energy difference between the two adiabatic states oscillates between 2.3 and 3.4 kcal/mol, which hints at an elliptical topography of the conical intersection.[155] Figure S5 in the Supporting Information shows that both the energies of the two states and the charge-transfer character of the ground state oscillate. This is due to the fact that while moving along the circle the electronic character of the ground state changes from diradical to charge-transfer and back. The MRCISD method also shows the correct behavior for a conical intersection. The energy-difference profile suggests that the topography of the MRCISD conical intersection is different from that of the CASSCF conical intersection. The individual state energies for the MRCISD method and the charge-transfer character of the ground state are shown in Figure S6 in the Supporting Information. The MRCISD+Q method does not yield the correct intersection topology because the Davidson correction affects only the energies but not the interstate couplings. This is why a vanishing $S_0$−$S_1$ energy gap is found for MRCISD+Q.

All ADC methods behave the same way: the three ADC methods shown in panel (a) reach a vanishing energy difference twice each, which is also true for the two SOS variants shown in panel (b). This is due to the fact that the $S_1$ state is described at the ADC level of theory, whereas the $S_0$ state is described at the

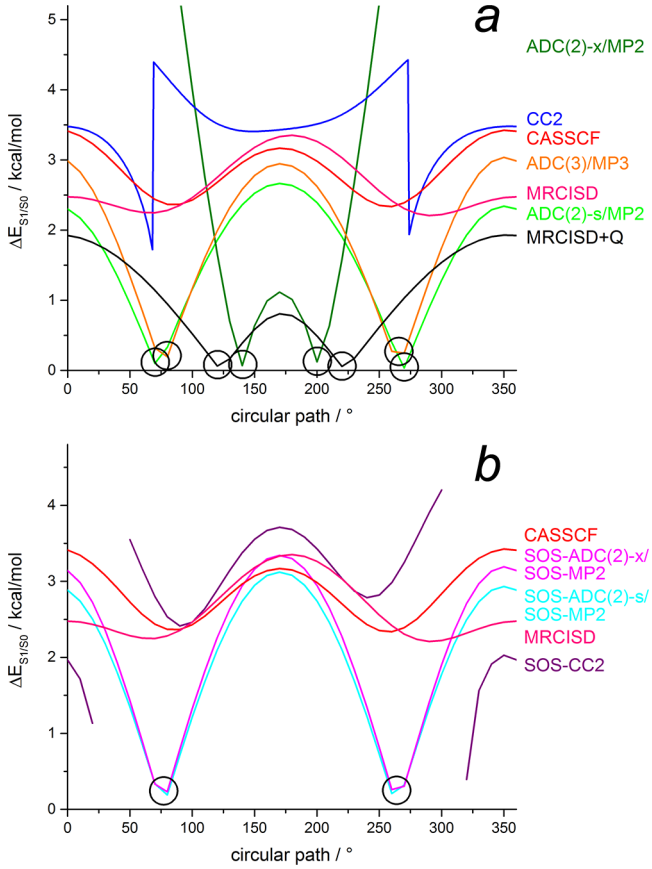


**Figure 9.** $S_1$−$S_0$ energy difference (in kcal/mol) along a circle centered around the surface crossing of PSB3. (a) Energy differences for the CC2 (blue), ADC(2)-s (green), ADC(2)-x (olive), and ADC(3) (orange) methods as well as for the CASSCF (red), MRCISD (pink), and MRCISD+Q (black) reference methods. (b) Energy differences for the SOS-CC2 (purple), SOS-ADC(2)-s (cyan), and SOS-ADC(2)-x (magenta) methods as well as for the reference methods. The approximate location of the surface crossing was determined for the response methods and for the MRCISD+Q method by locating the crossing point along the BLA scan (cf. full circles shown in Figure 4). For those methods that did not yield a crossing point in the original BLA scan, the BLA path was extrapolated for the determination of the crossing point. For the CASSCF and MRCISD methods, the optimized minimum-energy conical intersections were used instead. These approximate or exact geometries for the surface crossings were used for the construction of the 36 geometries in increments of 10° located on a circle spanned by the orthonormalized **g** and **h** vectors determined at the CASSCF level. For the CC2 method, 360 geometries were constructed in increments of 1°. A crossing of the two states along the circle results in a vanishing energy difference and is highlighted by black circles. The discontinuities observed for the SOS-CC2 method are due to a few points along the circle for which the calculations did not converge.

MP level of theory. The missing nonadiabatic coupling between $S_1$ and $S_0$ leads to a linear intersection topology, which presents in the form of two vanishing $S_0$−$S_1$ energy gaps along the circle. The complete absence of any interaction between the reference state and the response state for the ADC(2)-s method is also evident from Figures S10 and S11 in the Supporting Information: the charge-transfer character of the reference state remains constant, and the dipole moments of the two states barely vary.

While the CC2 method shows two distinct discontinuities, which result from the reference state and the response state switching energetic order, it nevertheless suggests empirically


DOI: 10.1021/acs.jctc.5b00022
J. Chem. Theory Comput. 2015, 11, 5758−5781

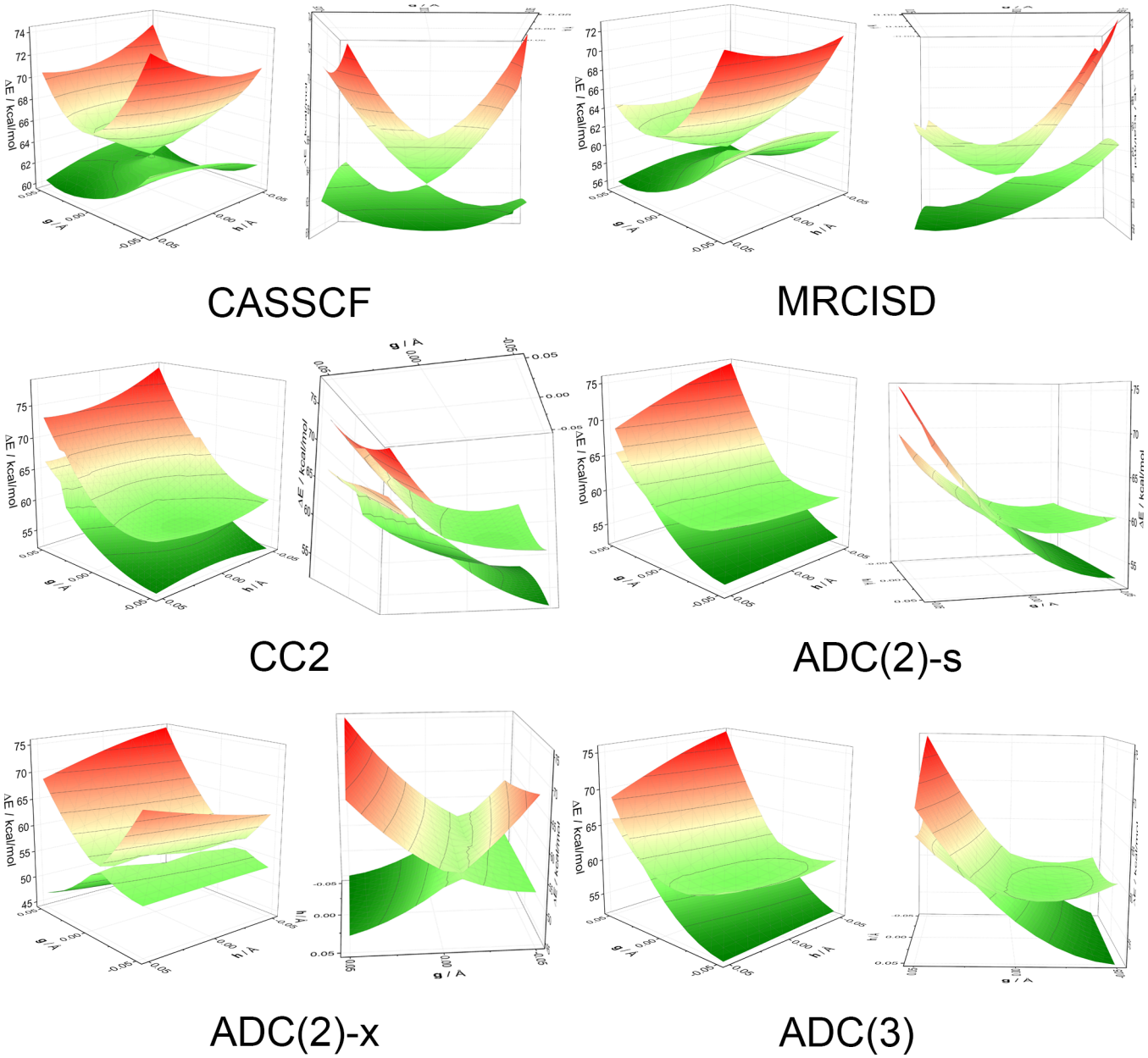


**Figure 10.** Energy profiles (in kcal/mol) of the $S_0$ and $S_1$ adiabatic potential-energy surfaces in the 2D branching space of the conical intersection of PSB3 (note that the energy scales are different for each plot). The **g** vector corresponds roughly to the BLA coordinate, whereas the **h** vector corresponds roughly to the isomerization coordinate (cf. Figure S1). The grids were constructed by displacing the geometry of the optimized minimum-energy conical intersection (in the case of CASSCF and MRCISD) or of the approximate surface crossing determined via the BLA scan shown in Figure 4 (in the case of the linear-response methods) up to 0.05 Å in each direction along the orthonormalized **g** and **h** vectors (which were determined at the CASSCF level except for MRCISD, for which we used the vectors determined at the MRCISD level). For each method, the plot is shown from two different perspectives. For the CC2 method, a roughly three times finer grid was used and a few points are missing due to nonconvergence.

that the CC2 method describes a seemingly true conical intersection due to the nonvanishing energy gap. The strong interaction between the reference and response states is also indicated by the large variation of the charge-transfer character of the reference state shown in Figure S8 in the Supporting Information. Figure S9 shows the strong variation in the dipole moments of the two states. Artifactual spikes at the points where the two states switch in energetic order are also observed. The variations in the charge-transfer character and in the dipole moments, which serve as diagnostics of the wave-function character, also suggest that the CC2 method describes continuously varying wave functions around the surface crossing, which is indicative of a conical intersection. For the SOS-CC2 method, we did not succeed in finding a radius for which we could converge the entire circular pathway (cf. Figure 9b). Close to the two areas along the circle where the excitation energy of the response state becomes negative, the SOS-CC2 method does not converge (in contrast to the CC2 method). However, also for the SOS-CC2 method the energy gap never vanishes.

The energy profiles along the circular paths of the $S_0$ and $S_1$ or for the reference and response states, respectively, which were used for the computation of the energy differences shown in Figure 9, are shown in Figures S5−S16 in the Supporting Information. The reader should note the switch in the energetic


DOI: 10.1021/acs.jctc.5b00022
J. Chem. Theory Comput. 2015, 11, 5758−5781

order between the reference and response states observed for the CC2 and ADC methods (cf. Figures S8, S10, and S12−S16). Also, for the CASSCF method, we compare the effects of constructing a circle around the surface-crossing point determined by the BLA scan (cf. Figure 4) and around the CASSCF-optimized minimum-energy conical intersection, which is shown in Figure S17. We also compare the effects of using the orthonormalized CASSCF or the orthonormalized MRCISD branching-space vectors for the CASSCF energy profiles along the circle. Finally, we compare the effect of different radii of 0.02 and 0.002 Å for the CASSCF energy profiles. The latter two comparisons are shown in Figure S18. The circular pathways obtained in these various ways yield qualitatively the same results as those shown in Figure 9.

**3.6. 2D Scans along the Branching Plane.** The energy profiles of the 2D potential-energy surfaces constructed in steps of 0.01 Å in the branching plane spanned by the two orthonormalized branching-plane vectors of the optimized $S_1/S_0$ conical intersection or approximate $S_1/S_0$ surface crossing of PSB3 are shown in Figure 10 for the various methods from two different perspectives. (The plots for the SOS variants of the CC2, ADC(2)-s, and ADC(2)-x methods are shown in Figure S19 in the Supporting Information.) The branching-plane vectors were determined at the CASSCF level of theory by optimizing the minimum-energy conical intersection (except for the MRCISD method, for which we used the MRCISD branching-plane vectors instead). The CASSCF method yields a peaked conical intersection of proper topology, that is, a true conical intersection, which exhibits a degeneracy inside the branching plane at a single point only. This is consistent with the correct dimensionality of a conical intersection of $3N - 8$. Upon distortion of the geometry of the conical intersection along the branching-space vectors, the energies of the intersecting potential-energy surfaces split. None of the other methods shown in Figure 10 yields such a peaked conical intersection. In contrast to the CASSCF conical intersection, the MRCISD conical intersection shows a sloped-intermediate topography. This is due to the shifting of the position of the curve crossing to higher BLA values, as already shown in Figure 4.

The charge-transfer character of the wave function of the $S_0$ and $S_1$ states computed at the MRCISD level is shown in Figure S20 in the Supporting Information. It shows the rapid transition of the ground-state wave-function character from a diradical character to a charge-transfer character at the conical intersection along the direction of the **g** vector (cf. Figure S20a and b) and the reversed behavior for the excited state (cf. Figure S20c). When followed adiabatically through the surface crossing, the ground and excited states exhibit an opposite wave-function character, that is, the ground state evolves from a diradical to a charge-transfer wave function, whereas the excited state evolves from a charge-transfer to a diradical wave function (cf. Figure S20d). This behavior is a manifestation of the so-called geometric-phase effect, which is the signature property of a true conical intersection.[156]

In Figure 10, the CC2 method shows a splitting of the energy along both the **g** and **h** vectors, although the branching of the two potential-energy surfaces is shallower than it is for MRCISD. It also shows a sloped-intermediate topography similar to MRCISD. As shown in Figure S19 in the Supporting Information, SOS-CC2 gives a qualitatively similar picture, although the splitting becomes even shallower. These observations confirm the conclusions drawn from the circular path around the surface crossing shown in Figure 9, which did not show a state crossing for the CC2 method, suggesting that this method yields a seemingly true $S_1/S_0$ conical intersection. However, note that both CC2 and SOS-CC2 show irregularities near the surface crossing, which, although difficult to spot in Figures 10 and S19, can be clearly observed along the circular path around the surface crossing shown in Figures 9, S8, and S14. Figure S21 in the Supporting Information shows the two CC2 potential-energy surfaces from Figure 10 divided up into the reference and response states. Analogously to what has been shown for the extended BLA scan in Figure 5, Figure S21 shows that the reference state becomes the adiabatic $S_1$ state in some regions of the branching plane (that is, it becomes higher in energy than the response state). Moreover, it is apparent from Figure S21 that numerous artifacts occur in the vicinity of the surface crossing, with the response state behaving particularly erratically. Interestingly, these artifacts do not occur along the **h** = 0.00 Å isoline, for which both the reference and response states behave smoothly. Since the center of this 2D plot is the crossing point determined via the BLA scan (cf. Figure 4), the **h** = 0.00 Å isoline corresponds to the picture shown in Figure 5a. (Note that for the generation of Figure 5a the pure BLA motion was used, whereas the nuclear-displacement vectors of the CASSCF-determined branching-plane vectors were used for the generation of the 2D scans; hence, the motion along the **g** vector can contain minor contributions from other molecular motions.) This behavior suggests that the artifacts are introduced by displacing the CC2 crossing point along the **h** vector, which corresponds to the isomerization motion of the central double bond of PSB3. Unfortunately, we cannot recognize any physical cause for these artifacts. The four frontier molecular orbitals HOMO − 1 to LUMO + 1, which are all $\pi$ orbitals, remain continuous (that is, they do not change in energetic order) throughout the entire 2D grid. The charge-transfer character of the CC2 reference state along the branching space is shown in Figure S22 in the Supporting Information. It shows that the wave-function character of the CC2 reference state changes twice from a strong charge-transfer character to a weaker charge-transfer character upon a full revolution around the surface crossing, which indicates a significant change in the wave function when traversing around the crossing point. However, one has to note that the reference state becomes the adiabatic $S_1$ state in some regions of the branching space, in which case the wave-function character of the excited state is depicted.

All ADC methods yield a linear topology for the surface crossing: the degeneracy is retained along the direction of the **h** vector. This observation confirms the conclusions drawn from the circular paths shown in Figure 9, which shows that the states cross twice. Thus, the ADC methods yield a $(3N - 7)$-dimensional intersection space and linear surface crossings. The reader should note that previous theoretical analyses concluded that ADC methods should be able to describe a conical intersection between excited states, whose excitation energies are obtained from a Hermitian Jacobi matrix, physically correctly.[42,86,87] Here, however, the $S_1/S_0$ surface crossing, which is computed with an ADC method, is, in fact, and as already mentioned in the Introduction, described at two different levels of theory: the response state is described at the ADC level of theory, whereas the reference state is described at the MP2 or MP3 level of theory instead. The description of the two intersecting potential-energy surfaces with two different electronic-structure methods, that is, one method for the description of the excited-state and another method for the description of the ground-state potential-energy surface, means


DOI: 10.1021/acs.jctc.5b00022
J. Chem. Theory Comput. 2015, 11, 5758−5781

that there is no coupling between the intersecting states. Therefore, the degeneracy is retained along the direction of the CASSCF-determined nonadiabatic-coupling vector (the **h** vector), and the $S_1/S_0$ surface crossings computed with ADC/MP methods present as linear intersections. The ADC(2)-x method exhibits potential-energy surfaces of reversed tilt compared to that of the other ADC methods because the energetic order of the diabatic states is reversed (cf. Figure 4). This leads to a surface crossing in the negative BLA region, where the curvature of the intersecting curves is also reversed compared to the positive BLA region (where all the other surface crossings are found).

The effect of using MRCISD branching-space vectors instead of CASSCF branching-space vectors for the construction of the 2D grids for the CASSCF, CC2, and ADC(2)-s methods is shown in Figure S23 in the Supporting Information. It is obvious that the differences are minor. This is rationalized by the comparison of the orthonormalized CASSCF and MRCISD branching-space vectors shown in Figure S1 of the Supporting Information: these vectors are, apart from their reversed sign, almost equal. Figure S23 also shows the 2D plot for the MRCISD+Q method, which shows the expected signs of irregularities close to the point of degeneracy: the degeneracy is not found for a single point only, but multiple points in close vicinity to the crossing point show a vanishing energy gap. These artifacts are, as already mentioned above, caused by the Davidson correction.

One may wonder whether it is appropriate to apply the branching-space vectors obtained at the CASSCF or MRCISD level for the approximate CC2 or ADC surface crossings to construct the circles and 2D grids around the surface crossing. In principle, these vectors have to be very similar to the method-specific CC2 or ADC branching-space vectors because at a conical intersection (or surface crossing in the case of ADC) one cannot observe an energy splitting along two (or one) nuclear-displacement vectors unless these vectors contain components of the exact branching-space vectors. Any nuclear displacement, which is not a component of a branching-space vector, moves the system along the intersection seam and thus no splitting of the degeneracy can be observed. If, for example, the CASSCF or MRCISD branching-space vectors were completely different from the method-specific CC2 branching-space vectors, then one would observe either a linear splitting or no splitting at all. While we have no means to directly compute the nonadiabatic-coupling vector for the CC2 method at the moment, we can, however, compute the gradient-difference vector to make a comparison to the CASSCF and MRCISD vectors. Thus, we computed the gradient-difference vector for the CC2 method by subtracting the reference-state energy gradient from the response-state energy gradient computed at the approximate point of surface crossing determined by the BLA scan. The result is shown in Figure 11. The obtained CC2 gradient-difference vector (cf. Figure 11c) agrees very well with one of the branching-space vectors obtained via the CASSCF and MRCISD optimizations of the minimum-energy conical intersection (cf. Figure 11a,b). Surprisingly, however, it agrees with the branching-space vector that was obtained as the nonadiabatic-coupling vector in both the CASSCF and MRCISD optimizations of the minimum-energy conical intersection. However, as has been shown in the seminal paper by Atchity, Xantheas, and Ruedenberg, the **g** and **h** vectors rotate, that is, exchange their character, upon a 90° rotation along a tiny loop around the conical intersection.[157] Since the optimization of a minimum-energy conical intersection, in general, never converges to the exact conical intersection, but instead close-by and thus on an imaginary loop around the exact conical intersection, it is a coincidence that both the CASSCF and MRCISD optimizations of the minimum-energy conical intersection ended up on a point close to the exact conical intersection where the **g** and **h** vectors exhibit the observed character. As a consequence, the fact that the CC2 gradient-difference vector compares to the nonadiabatic-coupling vector of CASSCF and MRCISD is merely coincidental.

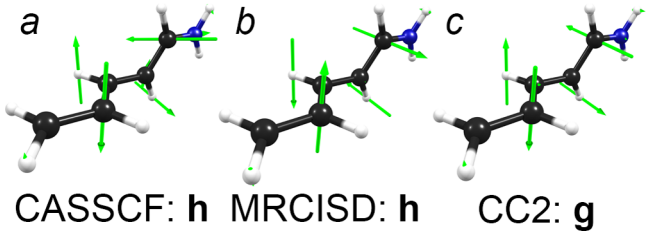


**Figure 11.** Comparison of the nonadiabatic-coupling vectors obtained from the optimization of the minimum-energy conical intersection at the (a) CASSCF and (b) MRCISD levels of theory, with the (c) CC2 gradient-difference vector computed for the surface-crossing geometry determined by the BLA scan (cf. Figure 4).

**3.7. $D_1$ and $D_2$ Diagnostics for the CC2 Method.** The $D_1$ diagnostic measures the extent of strong interaction of the Hartree−Fock reference wave function with singly excited determinants, whereas the $D_2$ diagnostic measures the extent of strong interaction of the Hartree−Fock reference wave function with doubly excited determinants.[158,159] Since CC2 is a single-reference method, it is, strictly speaking, adequate only for describing molecular systems with a single-reference ground state, that is, an electronic ground state that is dominated by a single determinant. A large $D_1$ or $D_2$ value indicates a strong multireference character of the electronic ground state and thus hints at the possibility that the CC2 method may not be appropriate to describe the system at hand. Köhn and Hättig concluded that a $D_1$ value of up to 0.15 and a $D_2$ value of 0.25 is acceptable for the CC2 method to be an adequate method for the description of a given electronic system.[41] The $D_1$ and $D_2$ diagnostics can be evaluated for any linear-response method and serve the purpose of detecting hidden multireference character in the reference wave function.

Figure 12 shows the values of the $D_1$ and $D_2$ diagnostics for the CC2 method along the branching space of the $S_1/S_0$ surface crossing. These two diagnostics overshoot the previously suggested trust regions[41] in large regions of the branching space. Low diagnostic values are found for the coordinate space generated by displacement of the geometry of the surface crossing along the **g** vector, which corresponds to the BLA motion. Large values are found for the coordinate space generated by displacement of the geometry of the surface crossing along the **h** vector, which roughly corresponds to the torsion motion of the central double bond.

To rationalize the behavior of the $D_1$ diagnostic for the CC2 method, we have to revisit some insight gained from CASSCF calculations.[27] We know from CASSCF calculations that at $TS_{CT}$ the electronic ground state consists almost purely of the closed-shell configuration, which constitutes the charge-transfer wave function at this geometry. When $TS_{CT}$ decays toward *cis*- or *trans*-PSB3 by introducing torsion around the central double bond, the closed-shell configuration mixes with the diradical configuration (cf. Figure 1B of ref 27). The introduction of this mixing with a singly excited determinant increases the multireference character


DOI: 10.1021/acs.jctc.5b00022
J. Chem. Theory Comput. 2015, 11, 5758−5781

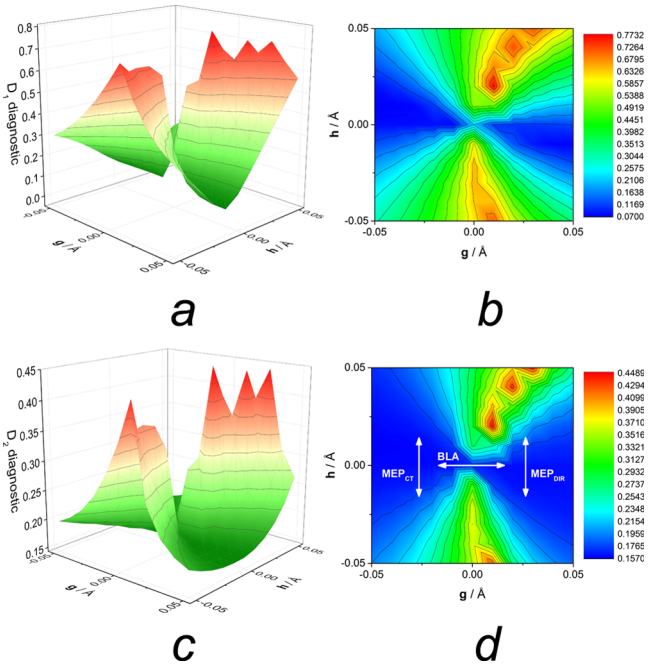


**Figure 12.** $D_1$ and $D_2$ diagnostics for the CC2 method in the 2D branching space of the surface crossing determined for the CC2 method. The values of the $D_1$ (a, b) and $D_2$ (c, d) diagnostics are shown as 2D (a, c) and contour (b, d) plots. The **g** vector corresponds roughly to the BLA coordinate, whereas the **h** vector corresponds roughly to the isomerization coordinate (cf. Figure S1). The arrows in part (d) indicate schematically which regions of the branching space conceptually correspond to the BLA, the $MEP_{CT}$, and the $MEP_{DIR}$ paths introduced earlier in Figures 4, 6, and 7.

of the ground state, which results in the sharp increase of the $D_1$ diagnostic for the CC2 method along the $MEP_{CT}$-like path in Figure 12b (cf. Figure 12d for a schematic drawing indicating the $MEP_{CT}$-like path). This increase in the multireference character of the CC2 reference state brings the CC2 method closer to the edge of its indended use, since the presence of a largely single-reference ground state is a prerequisite for a qualitatively reasonable description of the reference state with a single-reference linear-response method. We also know from CASSCF calculations that at $TS_{DIR}$ the electronic ground state consists purely of the diradical configuration (cf. Figure 1B of ref 27). When $TS_{DIR}$ decays toward *cis*- or *trans*-PSB3 by introducting a torsion motion, the diradical configuration mixes with the closed-shell configuration. The closed-shell configuration gains ever more weight en route to the planar minima before it dominates at *cis*- or *trans*-PSB3. Thus, $TS_{DIR}$ itself is of mostly single-reference character, yet the mixing in of the closed-shell configuration on the way toward the planar minima introduces a strong multireference character into the electronic ground state. This is why the $D_1$ diagnostic of the CC2 method also increases sharply along the $MEP_{DIR}$-like path in Figure 12b. The asymmetry observed in the contour plot of the $D_1$ diagnostic is due to the stronger multireference character of the $MEP_{DIR}$ path compared to that of the $MEP_{CT}$ path. Thus, the valley of acceptable $D_1$ values, that is, the blue region, on the right-hand side of Figure 12b is smaller than that on the left-hand side.

As for the $D_2$ diagnostic, it is known that the presence of diradical electronic states causes doubly excited determinants to be of considerable weight. In an earlier subsection, we have observed the dramatic overstabilization of $\Psi_{DIR}$ by the ADC(2)-x method along the BLA scan (cf. Figure 4), which shows that the diradical state (which is obtained as the response state) exhibits strong double-excitation character. Thus, the large values of the $D_2$ diagnostic for the CC2 method indicate the regions of the branching space that are characterized by a strong contribution of diradical character.

In summary, the CC2 method overshoots the currently recommended trust regions for the $D_1$ and $D_2$ diagnostics in large regions of the branching space of the $S_1/S_0$ surface crossing of PSB3. We elaborate on a possibly necessary reevaluation of the trust regions for the $D_1$ and $D_2$ diagnostics for the application to medium-sized organic molecules in the Discussion and Conclusions section.

It is evident that the behavior of both the $D_1$ and $D_2$ diagnostics is inversely correlated to the charge-transfer character of the CC2 reference state shown in Figure S22 in the Supporting Information. In regions of strong charge-transfer character, both diagnostics are found to have low values. In regions of weak charge-transfer character, both diagnostics are found to have large values. Figure S24 in the Supporting Information shows a 2D and a contour plot for the $\%T_2$ measure along the branching space of the surface crossing determined for the CC2 method. The $\%T_2$ measure indicates the percentage extent of double-excitation character of the linear-response description of an electronically excited state.[41] It is obvious that the picture given by the $D_2$ diagnostic shown in Figure 12c,d directly correlates to the picture given by the $\%T_2$ measure in Figure S24. In those regions of the branching space where the $D_2$ diagnostic indicates a strong interaction of the reference wave function with doubly excited configurations (which is an indication for the diradical state), the $\%T_2$ measure indicates that the description of the first response state involves a high percentage of double excitations (which is generally the case for the description of a diradical state).

Figure S25 in the Supporting Information shows the 2D plots of the $D_1$ and $D_2$ diagnostics for the ADC(2)-s/MP2 level of theory as well as the double-excitation character of the response state treated at the ADC(2)-s level (as measured by the $\%T_2$ measure). The $D_1$ diagnostic for the MP2 method shows only minor variations around the value of about 0.044 and thus slightly overshoots the trust region of up to 0.04 proposed by Janssen and Nielsen for an adequate description of the electronic ground state.[158] The $D_2$ diagnostic for the MP2 method shows only minor variations around the value of about 0.146 and is thus still within the acceptable range of up to 0.17 proposed by Janssen and Nielsen.[159] The $\%T_2$ measure shows that the double-excitation character of the response state treated at the ADC(2)-s level remains fairly low, giving a weight of double excitations ranging from 8.6 to 9.3%. It is noteworthy that all three values show only minor variations along the entire branching space.

**3.8. CC2 Gradient-Difference Vector along a Circular Path around the Surface Crossing.** To elucidate whether the CC2 surface crossing shows the characteristics of a true conical intersection, we checked whether the gradient-difference vector exhibits a change in character along a circular path around the surface crossing. As already mentioned above, the classic paper by Atchity, Xantheas, and Ruedenberg has shown that in the case of a true conical intersection the branching-plane vectors interact continuously and therefore exchange their character roughly every 90° upon a full revolution around the conical intersection.[157] The exchange in character of the branching-plane vectors around a surface crossing can thus be used as a signature test for a true conical intersection. We have computed


DOI: 10.1021/acs.jctc.5b00022
J. Chem. Theory Comput. 2015, 11, 5758−5781

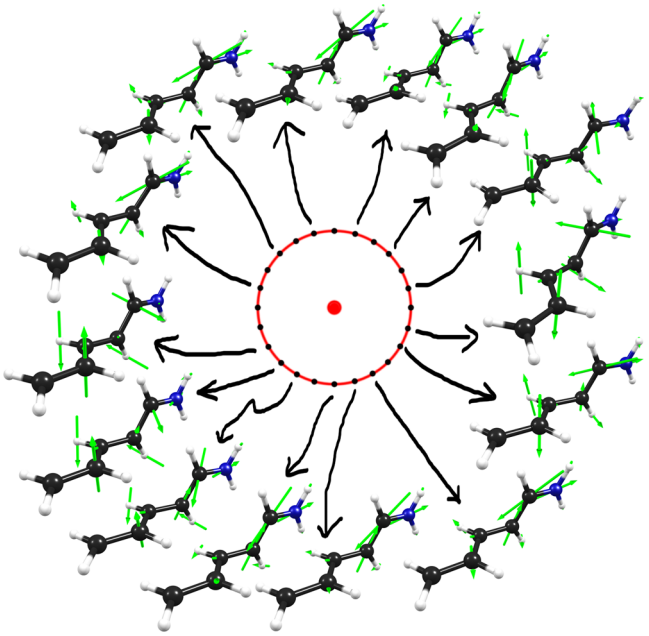

**Figure 13.** Depiction of the crossing point (thick red dot) and the circular path (red circle) around the crossing point from a top-down perspective. Molecular structures for which the CC2 gradient-difference vector was computed are shown by black dots. For selected structures, the gradient-difference vector is depicted by its nuclear-displacement vectors. The gradient-difference vector gradually changes in character from the BLA motion to the isomerization motion twice around the circle.

the gradient-difference vector with the CC2 method in steps of 15° along the circular path of 0.03 Å radius around the surface crossing. Figure 13 shows the point of surface crossing and the circular path constructed around it. The circular path was constructed in steps of 1°, and the energy profiles of the reference and the response states are shown in Figures 9 and S8. For selected structures, the nuclear-displacement vectors of the gradient-difference vector are shown in Figure 13. It is evident that for some structures the gradient-difference vector is clearly characterized by the isomerization motion (as already shown in Figure 11), but it gradually evolves into the bond-length alternation (BLA) motion before it evolves back into the isomerization motion. In between, it can exhibit a combinatorial character between the BLA and the isomerization motion. As a verification, we have performed the same procedure on a tighter circular path of 0.015 Å radius on which we computed the gradient-difference vector in steps of 10° (not shown). This gave the same results as those shown and discussed above. This behavior of the CC2 gradient-difference vector shows that the linear-response CC2 method apparently describes the $S_1/S_0$ surface crossing as a true conical intersection. We elaborate on this finding in the Discussion and Conclusions section.

As a byproduct of this test, we have obtained the CC2 nonadiabatic-coupling vector in an indirect manner: when the gradient-difference vector exchanges its character, the newly found character constitutes the nonadiabatic-coupling vector. This CC2 nonadiabatic-coupling vector compares well with the gradient-difference vector obtained by the CASSCF and MRCISD methods (cf. Figure S1 in the Supporting Information).

For comparison, we have performed the same test also for the ADC(2)-s method. We have computed the ADC(2)-s/MP2 gradient-difference vector along the circular path shown in Figure 9 in increments of 10° (not shown). This has revealed that the gradient-difference vector exhibits a clear and unchanging BLA motion along the entire circular path (that is, one cannot spot any changes). This indicates that the nonadiabatic coupling between the MP2 reference state and the first ADC(2)-s response state is zero.

**3.9. Approximate Geometry Optimization of Minimum-Energy Conical Intersections Using the CC2 and ADC(2)-s Methods.** Levine, Coe, and Martínez have developed an algorithm and the program CIOpt that allows the approximate optimization of minimum-energy conical intersections with any electronic-structure method capable of providing the energy of electronically excited states.[148] Most importantly, CIOpt does not require the nonadiabatic-coupling vector **h**, which cannot be analytically computed for ADC or CC2 at present, and therefore can conveniently provide an approximate geometry for a minimum-energy conical intersection. The combination of the program CIOpt with the CC2 or ADC(2)-s methods offers an efficient route to optimize approximate minimum-energy conical intersections for medium-sized molecules without having to use a method based on an active space such as the CASSCF, MRCI, or the semiempirical OMx/MRCI method.[15,160] This has been recently demonstrated by the optimization of the geometries of conical intersections for adenosine,[96] a model dipeptide,[161] the naturally occurring UV filter kynurenine,[97] an aminopurine−water cluster,[104] a dimer of azaindole,[72] and an adenine−water cluster.[116] We use this opportunity to compare the geometries of the $S_1/S_0$ minimum-energy conical intersection for the photoisomerization process in PSB3 optimized at the CC2 and ADC(2)-s/MP2 levels with the CASPT2- and MRCISD-optimized minimum-energy conical intersections. This serves to assess the quality of such approximate geometry optimizations of surface crossings employing the CC2 or ADC(2)-s/MP2 method.

Figure 14 shows the structural parameters of the minimum-energy surface crossings of PSB3 optimized with the CC2 and the ADC(2)-s/MP2 methods compared to literature values,[4,9,15] which were obtained by optimization at the CASPT2 and MRCISD levels of theory. All methods agree well in the geometrical parameters of the allyl fragment of PSB3, whereas striking differences are found in the iminium fragment. Among the five methods, deviations in the C1═C2 bond length of more than 0.05 Å can be found. If one takes the MRCISD-optimized structure obtained by Nikiforov et al. as a reference,[15] the structures obtained at the CC2 and ADC(2)-s/MP2 levels agree, however, surprisingly well. While the deviations in the allyl fragment are negligible, the largest deviations found in the iminium fragment amount to 0.02 Å. For completeness, we mention that the $S_1-S_0$ energy gaps are 1 m$E_h$ at the approximate CC2 intersection and 0.8 m$E_h$ at the approximate ADC(2)-s/MP2 intersection. A superposition of the five structures is shown in Figure S26 in the Supporting Information. This indicates that the CC2 and the ADC(2)-s/MP2 methods offer a cost-effective and convenient approach for optimizing minimum-energy surface crossings of organic molecules.

An alternative approach for the optimization of minimum-energy conical intersections is the updated branching-plane method introduced by Maeda, Ohno, and Morokuma.[162] This method is especially interesting for linear-response methods, since it not only allows the optimization of the geometry of the surface crossing but also provides approximate branching-space vectors, which cannot yet be analytically computed for many


DOI: 10.1021/acs.jctc.5b00022
J. Chem. Theory Comput. 2015, 11, 5758−5781

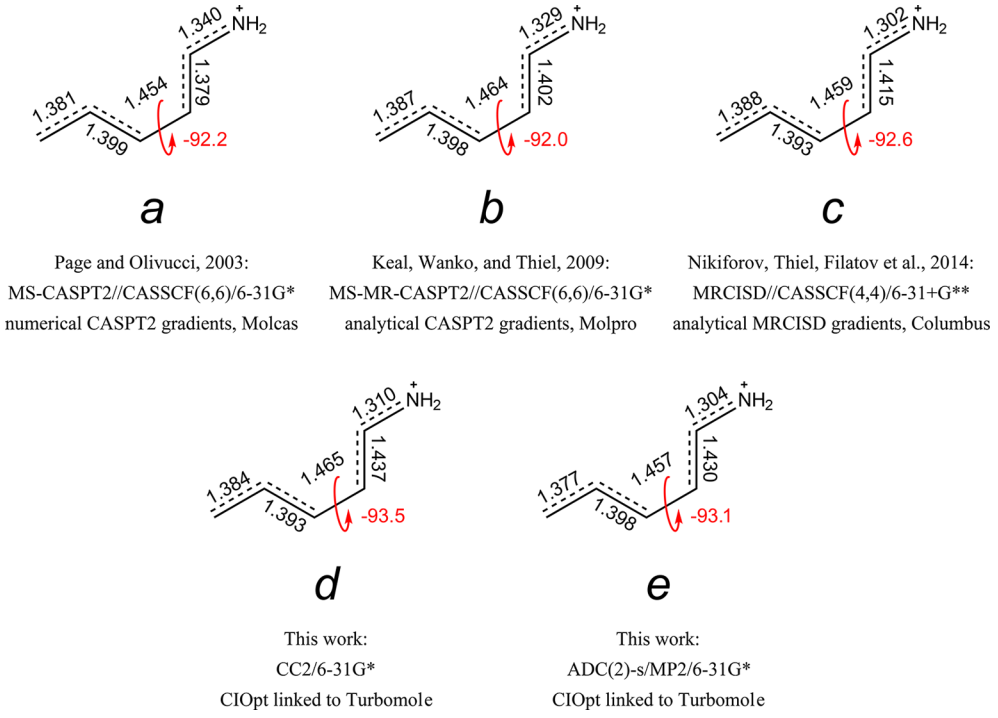


**Figure 14.** Comparison of geometries for the minimum-energy $S_1/S_0$ conical intersection of PSB3 optimized by Page and Olivucci with the CASPT2 method (a),[4] by Keal, Wanko, and Thiel with the CASPT2 method (b),[9] by Nikiforov, Gamez, Thiel, Huix-Rotllant, and Filatov with the MRCISD method (c),[15] with the CC2 method as part of this work (d), and with the mixed ADC(2)-s/MP2 method as part of this work (e).

linear-response methods. Therefore, the updated branching-plane method offers a route to obtain a nonadiabatic-coupling vector for CC2 $S_1/S_0$ surface crossings and for excited-state ADC(2) surface crossings. Unfortunately, we do not have access to the program package containing the updated branching-plane algorithm yet, but we aim to perform these potentially insightful computations soon and will report on these results in a future benchmark study.

## 4. DISCUSSION AND CONCLUSIONS

In this work, we have assessed the performance of the linear-response CC2 and ADC methods for ground- and excited-state reaction paths, for the description of the topography and topology of the $S_1/S_0$ surface crossing, and for the geometry optimization of the surface crossing of PSB3.

In terms of recovering the system's dynamical correlation energy, we have shown that among the tested linear-response methods the CC2 and the ADC(3) methods perform best, as shown by the energy profiles along the BLA, $MEP_{CT}$, and $MEP_{DIR}$ pathways, which run fairly close to the energy profiles of the MRCISD+Q method. The typical deviation amounts to a few kcal/mol, although we have shown that the $S_1$ composite path exhibits deviations of more than 10 kcal/mol for the ADC(3) method. For the ground-state energy profiles, we have also shown that the MP2 method performs surprisingly well (given by the ground-state description for the ADC(2) methods). As far as qualitative reaction profiles along excited-state potential-energy surfaces are concerned, the CC2, ADC(2)-s, and ADC(3) methods show satisfying parallelity to the MRCISD+Q energy profiles. We have to point out that our results cannot be generalized because the excited-state reaction paths of PSB3 are dominated by wave functions of either diradical or charge-transfer character.

The ADC(2)-x method has been shown to overstabilize the energy of the excited state along all explored pathways. This well-known phenomenon is rooted in the inclusion of double excitations at first order of perturbation theory in the ADC(2)-x method, which leads to a lowering of double-excitation contributions to electronically excited states; thus, the energy of excited states is usually severely underestimated. However, it was also shown that the SOS variant of ADC(2)-x, SOS-ADC(2)-x, partially remedies this shortcoming, a property that was intended for this variant by design.[87,132] Other variants of ADC(2) have been proposed by Helmich and Hättig that remedy the problems inherent to ADC(2)-x.[89]

The investigation of the $S_1/S_0$ surface-crossing topology of the CC2 method has revealed some surprising results. Unexpectedly, the CC2 and SOS-CC2 methods yield a seemingly true $S_1/S_0$ conical intersection. Previous theoretical analysis by Hättig[42] and by Köhn and Tajti[147] has shown that the non-Hermitian theoretical foundation of linear-response CC2 yields a branching space of the dimensionality $3N - 7$ or $3N - 9$ *for surface crossings between excited states*, for example, for $S_2/S_1$ or $S_3/S_2$ surface crossings. This is opposed to the correct dimensionality of $3N - 8$, which is obtained only for the special case of a symmetric Jacobi matrix (in CC2 linear-response theory, the eigenvalues of the electronic Jacobian correspond to the poles of the polarization propagator and thus to the desired excitation energies).[42,147] As a single-reference method, CC2 should, in principle, not converge in close vicinity of a surface crossing between the electronic ground state and an electronically excited state because an $S_1/S_0$ surface crossing shows strong multi-reference character in the electronic ground state.[42,147] For this reason, the CC2 method is expected to break down or, in other words, never converge in the vicinity of an $S_1/S_0$ surface crossing. To our knowledge and possibly as a consequence of the above, a case such as we present here, that is, the analysis of the


DOI: 10.1021/acs.jctc.5b00022
J. Chem. Theory Comput. 2015, 11, 5758−5781

dimensionality of an approximate CC2 $S_1/S_0$ surface crossing, has not yet been considered, neither computationally nor theoretically. Herein, however, we have shown that for practical purposes the CC2 equations can converge in close vicinity of a surface crossing. This is possibly due to the fact that the surface-crossing points determined along the BLA scan are not perfect crossings, that is, they do not show an exact degeneracy. The approximate CC2 surface crossing determined via the BLA scan, for example, exhibits an energy gap of 0.2 m$E_h$ so that the critical breakdown region, in which the energy gap would be even smaller and the CC equations would not converge, has not been reached yet. (The energy gap of the approximate CC2 minimum-energy conical intersection optimized with the Levine−Coe−Martínez method[148] using standard settings is a little larger: 1 m$E_h$. This is why we used the crossing point determined via the BLA scan for the construction of the circular path and the 2D scan along the branching plane.)

In this work, we have presented several pieces of computational evidence of the linear-response CC2 method describing a true conical intersection for an $S_1/S_0$ surface crossing. Since the CC2 method is constructed by a linear-response formalism, an $S_1/S_0$ surface crossing corresponds to a surface crossing between the reference state and the first response state. The circular path around the CC2 surface crossing has shown that the energy gap between the reference state and the first response state never vanishes. This is the first indication that CC2 describes this surface crossing as a true conical intersection. (A linear intersection would present in the form of two vanishing energy gaps along such a circular path.) As the energy-difference profile (cf. Figure 9) and the energy profiles of the individual states (cf. Figure S8) show, two regions along the circular path are found in which the reference and first response states switch in energetic order. These regions are characterized by artifactual jumps in energy, but these are, however, very narrow. The variation in the charge-transfer character of the CC2 reference state along the circular path (cf. Figure S8) suggests that the electronic nature of the reference state changes, as is expected around a conical intersection. The analysis of the dipole moments of the two intersecting states along the circular path (cf. Figure S9) also shows a clear variation in the nature of the states along the circular path. However, the dipole moments also exhibit artifactual spikes. The second and most obvious piece of computational evidence is the presentation of the 2D scan along the branching space of the $S_1/S_0$ surface crossing. It is evident that the CC2 method yields a double-cone topology (cf. Figure 10). This hints at the existence of a nonvanishing nonadiabatic coupling between the reference state and the first response state. The analysis of the reference and the response states along the branching space shows a number of artifactual energy jumps and switches in energetic order (cf. Figure S21). However, when the energies are ordered in an adiabatic manner, the picture appears to be smoother, although artifacts are still visible (cf. Figure 10). The analysis of the charge-transfer character of the reference state along the branching plane again shows a clear variation when traversing around the surface crossing, a behavior that is characteristic of a conical intersection (cf. Figure S22). The third piece of computational evidence was given by the computation of the CC2 gradient-difference vector along the circular path around the surface crossing (cf. Figure 13). As already mentioned in the Results section, Ruedenberg and co-workers have shown that the branching-plane vectors continuously exchange their character when traversing along a closed loop around a conical intersection. Roughly every 90°, the gradient-difference vector is expected to take on the character of the nonadiabatic-coupling vector and vice versa.[157] Our computation of the CC2 gradient-difference vector along the circular path has shown how this vector gradually evolves from a BLA motion into a torsion motion and back. We have verified this by repeating the procedure along a circular path of smaller radius. This behavior can be understood as computational proof that a non-negligible nonadiabatic coupling indeed exists for the reference-state/response-state surface crossing at the CC2 level. When the character of the gradient-difference vector changes and takes on the character of the nonadiabatic-coupling vector, the nature of the nonadiabatic-coupling vector, which we have no means to compute directly at the moment, becomes apparent. In this way, we have computed the nonadiabatic-coupling vector for the CC2 method in an indirect manner. Both CC2 branching-plane vectors obtained in this way compare well with the vectors obtained via the geometry optimization of the minimum-energy conical intersection at the CASSCF and the MRCISD levels (cf. Figures 11 and S1). For comparison, we have repeated the procedure for the ADC(2)-s method, for which we found that the gradient-difference vector retains its character along the entire circular path. This shows that for a reference-state/response-state surface crossing a second branching-plane vector does not exist at the ADC(2)-s/MP2 level of theory.

As mentioned above, we have presented several pieces of computational evidence for the linear-response CC2 method describing a true conical intersection for surface crossings between the reference state and the first response state. By testing the behavior of the gradient-difference vector along a circular path around the surface crossing, which provides strong computational evidence for the correct description of the surface crossing as a true conical intersection, we have revealed the character of the nonadiabatic-coupling vector. This vector describes the vibronic coupling between the reference state and the first response state in the vicinity of the $S_1/S_0$ conical intersection. The finding of a nonvanishing nonadiabatic coupling between these two states deserves further elaboration. Christiansen has presented a derivation of the expressions for the nonadiabatic coupling-matrix elements between different types of states in linear-response coupled-cluster theory.[163] These expressions comprise reference-state/response-state couplings as well as couplings between response states (that is, between excited states). The expressions derived by Christiansen are valid in a general way for any linear-response coupled-cluster method. For the reference-state/response-state couplings, which apply to the case discussed herein, Christiansen has stated that these are, in general, nonvanishing.[163] To our knowledge, it has not been verified that the approximations introduced by the CC2 model[38] leave this fact unchanged, that is, that for the CC2 method the nonadiabatic coupling-matrix elements between the reference state and the first response state can be nonvanishing. A theoretical demonstration that this is the case is beyond the scope of this work and shall remain the focus of future studies. Herein, we have presented convincing computational evidence that the nonadiabatic coupling between the reference state and the first response state in CC2 linear-response theory is, indeed, nonvanishing. However, compared to the splitting of the potential-energy surfaces at the conical intersection found for the MRCISD method, it seems that the magnitude of the splitting is strongly underestimated by the CC2 method. (On a sidenote, we mention that the linear-response CCSD method behaves analogously to the CC2 method along the circular path around the surface crossing and along the 2D scan in the


DOI: 10.1021/acs.jctc.5b00022
J. Chem. Theory Comput. 2015, 11, 5758−5781

branching space. This is demonstrated in Figure S27 in the Supporting Information.)

The signature property of a true conical intersection is the geometric-phase effect, which is the only unambiguous proof for a true conical intersection and which states that a wave function changes sign when traversing along a closed loop around a conical intersection.[141,143,144,156] Unfortunately, we see no means to prove the geometric-phase effect computationally, since this requires the evaluation of an adiabatic wave function along a closed loop around the conical intersection. A linear-response method, however, does not provide a wave function for a response state but only for the reference state. Due to the switching of the energetic order of the reference and response states in some regions around the surface crossing, we see no means to evaluate an adiabatic CC2 wave function along a closed loop around the surface crossing. However, while we see no means to analyze the wave function directly, we have analyzed two properties that provide an indication of the wave-function character, namely, the charge-transfer character of the reference state obtained by Mulliken charges (cf. Figure S8) as well as the dipole moments of both the reference and response states (cf. Figure S9). The variations observed in these two properties suggest that the geometric-phase condition is fulfilled by the linear-response CC2 method for the case of a surface crossing between the reference state and the first response state.

The above notwithstanding, we have also shown that the CC2 method can exhibit many artifactual jumps in energy and sudden switches in the energetic order of the reference state and the first response state. We have observed such artifacts for the energy, the Mulliken charges, and the dipole moments of both states along the BLA scan, the circular path around the surface crossing, and along the 2D scan in the branching plane. While for static explorations such shortcomings can be acceptable, such artifacts can have undesirable consequences in molecular-dynamics simulations and could possibly lead to incorrect results. It should also be mentioned that such artifacts are not at all observed for the ADC methods, which is due to the complete lack of interaction between the reference state and the first response state for these methods.

Apart from the surprising behavior of the CC2 method around an $S_1/S_0$ surface crossing, we have demonstrated the more straightforward property of the ADC methods to yield linear surface crossings. This is obviously due to the description of the intersecting $S_1$ and $S_0$ states at different levels of theory, that is, at the ADC level for the $S_1$ state and at the MP level for the $S_0$ state. The linear topology of the branching space of the ADC surface crossing is, therefore, due to the nonexistent coupling between the MP and ADC levels of theory. The constant charge-transfer character of the reference state along the circular path around the surface crossing as well as the barely changing dipole moments of the two states (cf. Figures S10 and S11) further show that the reference state and the first response state do not interact at all. Similar to our results obtained at the CC2 level, we have shown that convergence of ADC methods (for which the electronic ground state is described by the MP2 or MP3 method) can be achieved for an $S_1/S_0$ surface crossing, which may, again, be due to the energy gap still present at this intersection determined via the BLA scan (which amounts to 0.4 m$E_h$ at the ADC(2)-s level). (From our experience in applying the CC2 and ADC(2)-s methods to many different systems, we can say that in the vicinity of surface crossings such convergence problems almost never occur for ADC, whereas for CC2 these do occur quite regularly.) Theoretical derivations available in the literature state that ADC methods should be able to correctly describe the topology of conical intersections between excited states (that is, between two response states) due to their Hermitian formulation.[42,86,87]

In summary, the exploration of the branching space of an $S_1/S_0$ conical intersection with the CC2 and ADC linear-response methods has pushed these methods toward the boundaries, or even beyond, of their intended purpose. Therefore, such explorations can be problematic with the two methods: the ADC method is unable to describe the correct topology because, due to the mixed ADC/MP description of an $S_1/S_0$ surface crossing, it yields only linear intersections. Unexpectedly, though, we found that the CC2 method yields seemingly conical $S_1/S_0$ intersections, yet it is prone to artifacts in the vicinity of surface crossings, and, in our experience, it can break down. This does not mean that one cannot use these methods for the static exploration of photochemical reaction paths. However, the occurrence of numerous artifacts around the surface crossing in the case of CC2 and the incorrect description of the topology of the surface crossing in the case of ADC/MP may have consequences for nonadiabatic molecular-dynamics simulations in the critical step of the radiationless deactivation of the $S_1$ excited state to the electronic ground state. Plasser et al. have previously reported on the unsuitability of CC2 for surface-hopping molecular-dynamics simulations due to numerical instabilities arising from the non-Hermitian formulation of CC2.[110] They have also commented on possible shortcomings of the ADC(2)-s method for the $S_1 \rightarrow S_0$ deactivation step in the simulation process, which could arise from the incorrect description of the $S_1/S_0$ surface-crossing topology.[110]

The above-mentioned problems notwithstanding, both the CC2 and ADC methods can be useful for optimizing approximate minimum-energy conical intersections by using the program CIOpt[148] interfaced with CC2 and ADC quantum-chemistry codes. The deviations in bond lengths from an MRCISD-optimized minimum-energy conical intersection of PSB3 did not exceed 0.02 Å. A benchmark study for assessing the quality of the geometries and relative energies of such CC2 and ADC(2)-s/MP2 optimized minimum-energy conical intersections compared to multireference results of a range of small- and medium-sized organic molecules is already under way.

The study of the $D_1$ and $D_2$ diagnostics as well as the $\%T_2$ measure along the branching space of the conical intersection indicates that the CC2 method overshoots the currently recommended trust regions for the $D_1$ and $D_2$ diagnostics along almost the entire branching space in the vicinity of the surface crossing. The $D_1$ diagnostic for the ADC(2)-s/MP2 method has indicated that this method exhibits a strong multireference character of the electronic ground state for the entire region around the conical intersection, which the MP2 method is supposedly unable to describe. The optimization of the minimum-energy conical intersection has shown, however, that the structures obtained with the CC2 and ADC(2)-s/MP2 methods are reasonable compared to high-level multireference results. Due to the above, the currently recommended trust regions of the $D_1$ and $D_2$ diagnostics for the CC2 and ADC(2)-s/MP2 methods call for some concluding remarks. Köhn and Hättig recommended to increase the trust region of the $D_1$ diagnostic from the value of 0.05 initially proposed by Janssen and Nielsen for CCSD[158] to 0.15 for CC2[41] and of the $D_2$ diagnostic from the value of 0.18 also proposed by Janssen and Nielsen for CCSD[159] to 0.25 for CC2.[41] Janssen and Nielsen considered mainly inorganic di-, tri-, and four-atomic molecules when recommending the trust regions for their newly proposed



DOI: 10.1021/acs.jctc.5b00022
J. Chem. Theory Comput. 2015, 11, 5758−5781

diagnostics,[158,159] whereas Köhn and Hättig considered similar molecules for their recommendation, yet among them a few small organic molecules.[41] Given our findings, we reinforce the suggestion of Plasser et al., who stated that the currently recommended trust regions for the $D_1$ and $D_2$ diagnostics (that is, the values recommended by Köhn and Hättig),[41] which are based on test sets lacking any aromatic molecules, might not be adequate anymore.[110] Plasser et al. pointed out that even adenine, whose excited states have been shown to be well-described by CC2[50,164] and ADC(2)-s,[88] exceeds these trust regions.[110] For these reasons, it might be worthwhile to perform a new benchmark study in the future that aims at recommending new trust regions for the $D_1$ and $D_2$ diagnostics for the application of CC2 and ADC methods to medium-sized organic molecules.

While the CC2 method is nowadays established for studying the energies, reaction paths, and properties of electronically excited states of organic molecules, the ADC methods have been used much less frequently for this purpose. However, in the current benchmark study, we find that ADC methods are, after taking into account the described limitations, useful for future applications in organic photochemistry. The ADC(2)-s method offers an efficient approach for the study of electronically excited states and shows favorable properties in comparison to those of CC2, that is, its Hermitian formulation, its compactness, as well as its slightly higher computational efficiency. The description of the electronic ground state by the MP method can be an advantage in some cases. If higher accuracy is needed, the ADC(3) method offers a significantly more affordable way to treat single-reference problems in molecular photochemistry than its much costlier counterpart CC3. As we have shown on multiple occasions in this work, these methods can even be used for regions of non-negligible ground-state multireference character. Another advantage of both CC and ADC methods is their "use-as-is" functionality, which means that the user typically need not set any parameters but select only a basis set. This makes the ADC method a worthwhile alternative, if the molecular size allows its use, to the widely used linear-response TDDFT method.

## ■ ASSOCIATED CONTENT

### Supporting Information

The Supporting Information is available free of charge on the ACS Publications website at DOI: 10.1021/acs.jctc.5b00022.

Comparison of CASSCF- and MRCISD-optimized minimum-energy conical intersections and the corresponding orthonormalized branching-space vectors. $S_1$ energy profiles along the $MEP_{CT}$ and $MEP_{DIR}$ pathways. Energy profiles along the composite CASPT2 $S_1$ path. $S_0-S_1$ energy gaps at five geometries along the composite CASSCF $S_1$ path. $S_0$ and $S_1$ or reference- and response-state energies, respectively, along the circular path around the conical intersection for the CASSCF, the MRCISD, the CC2, and the ADC(2)-s methods including the $S_0$/reference-state charge-transfer character. Dipole moments of the reference and the response states for the CC2 and the ADC(2)-s methods along the circular path around the surface crossing. Reference- and response-state energies along the circular path around the surface crossing for all remaining methods. Comparison of CASSCF circular paths created around conical-intersection points located by using different radii and by using CASSCF and MRCISD branching-space vectors. 2D plots of the $S_0$ and $S_1$ energies for the SOS variants of CC2, ADC(2)-s, and ADC(2)-x along the branching space. 2D plots of the charge-transfer character of the MRCISD $S_0$ and $S_1$ wave functions and 2D and contour plot of the charge-transfer character of the CC2 reference state along the branching space. 2D plots of the reference- and the response-state energies for the CC2 method along the branching space. 2D plots of the CASSCF, MRCISD, CC2, and ADC(2)-s potential-energy profiles along the branching space constructed with MRCISD branching-plane vectors. 2D and contour plot of the $\%T_2$ measure along the branching space for the CC2 method. 2D plots of the $D_1$ and $D_2$ diagnostics and the $\%T_2$ measure along the branching space for the ADC(2)-s method. Superposition of the five geometries for the $S_1/S_0$ surface crossing determined by optimization or approximate optimization. Energy profiles of the reference state and the response state along the circular path around the surface crossing and along the 2D scan along the branching space for the linear-response CCSD method. Energy profiles of SCS variants of CC2 and ADC(2)-s available in Turbomole compared to SOS-CC2, CC2, SOS-ADC(2)-s, and ADC(2)-s along the BLA, the $MEP_{CT}$, the $MEP_{DIR}$, and the composite $S_1$ CASSCF pathways as well as the circular paths around the surface crossing. Cartesian coordinates of the CASSCF-, MRCISD-, CC2- and ADC(2)-s/MP2-optimized minimum-energy conical intersections. (PDF)

## ■ AUTHOR INFORMATION


### Corresponding Authors

*(D.T.) E-mail: tuna@kofo.mpg.de.
*(T.A.) E-mail: tadeusz.andruniow@pwr.wroc.pl.
*(A.D.) E-mail: andreas.dreuw@iwr.uni-heidelberg.de.
*(M.O.) E-mail: molivuc@bgsu.edu.

### Present Address

∇(I.S.) The Fritz Haber Research Center for Molecular Dynamics, Institute of Chemistry, The Hebrew University of Jerusalem, Jerusalem 91904, Israel.



### Funding

D.L. acknowledges support by the Heidelberg Graduate School "Mathematical and Computational Methods for the Sciences" (GSC 220). Ł.W. and T.A. acknowledge a statutory activity subsidy from the Polish Ministry of Science and Higher Education for the Faculty of Chemistry of Wrocław University of Technology. M.O. is grateful to the National Science Foundation under grants no. CHE-1152070 and CHE-1551416 and to the Human Frontier Science Program Organization under grant no. RGP0049/2012CHE09-56776.


### Notes

The authors declare no competing financial interest.

## ■ ACKNOWLEDGMENTS


D.T. is grateful to Walter Thiel for his support and to Alexander Nikiforov for repeating the MRCI MECI optimization with our parameters.


## ■ REFERENCES


(1) Garavelli, M.; Celani, P.; Bernardi, F.; Robb, M. A.; Olivucci, M. The $C_5H_6NH_2^+$ Protonated Shiff Base: An *Ab Initio* Minimal Model for Retinal Photoisomerization. *J. Am. Chem. Soc.* **1997**, *119*, 6891−6901.




DOI: 10.1021/acs.jctc.5b00022
*J. Chem. Theory Comput.* 2015, 11, 5758−5781

(2) Garavelli, M.; Bernardi, F.; Robb, M. A.; Olivucci, M. The Short-Chain Acroleiniminium and Pentadieniminium Cations: Towards a Model for Retinal Photoisomerization. A CASSCF/PT2 Study. *J. Mol. Struct.: THEOCHEM* **1999**, *463*, 59−64.
(3) Sinicropi, A.; Migani, A.; De Vico, L.; Olivucci, M. Photoisomerization Acceleration in Retinal Protonated Schiff-Base Models. *Photochem. Photobiol. Sci.* **2003**, *2*, 1250−1255.
(4) Page, C. S.; Olivucci, M. Ground and Excited State CASPT2 Geometry Optimizations of Small Organic Molecules. *J. Comput. Chem.* **2003**, *24*, 298−309.
(5) Migani, A.; Robb, M. A.; Olivucci, M. Relationship Between Photoisomerization Path and Intersection Space in a Retinal Chromophore Model. *J. Am. Chem. Soc.* **2003**, *125*, 2804−2808.
(6) Fantacci, S.; Migani, A.; Olivucci, M. CASPT2//CASSCF and TDDFT//CASSCF Mapping of the Excited State Isomerization Path of a Minimal Model of the Retinal Chromophore. *J. Phys. Chem. A* **2004**, *108*, 1208−1213.
(7) Aquino, A. J. A.; Barbatti, M.; Lischka, H. Excited-State Properties and Environmental Effects for Protonated Schiff Bases: A Theoretical Study. *ChemPhysChem* **2006**, *7*, 2089−2096.
(8) Sumita, M.; Ryazantsev, M. N.; Saito, K. Acceleration of the *Z* to *E* Photoisomerization of Penta-2,4-dieniminium by Hydrogen Out-of-Plane Motion: Theoretical Study on a Model System of Retinal Protonated Schiff Base. *Phys. Chem. Chem. Phys.* **2009**, *11*, 6406−6414.
(9) Keal, T. W.; Wanko, M.; Thiel, W. Assessment of Semiempirical Methods for the Photoisomerisation of a Protonated Schiff Base. *Theor. Chem. Acc.* **2009**, *123*, 145−156.
(10) Mori, T.; Nakano, K.; Kato, S. Conical Intersections of Free Energy Surfaces in Solution: Effect of Electron Correlation on a Protonated Schiff Base in Methanol Solution. *J. Chem. Phys.* **2010**, *133*, 064107.
(11) Valsson, O.; Filippi, C. Photoisomerization of Model Retinal Chromophores: Insight from Quantum Monte Carlo and Multiconfigurational Perturbation Theory. *J. Chem. Theory Comput.* **2010**, *6*, 1275−1292.
(12) Malhado, J. P.; Hynes, J. T. Photoisomerization for a Model Protonated Schiff Base in Solution: Sloped/Peaked Conical Intersection Perspective. *J. Chem. Phys.* **2012**, *137*, 22A543.
(13) Filatov, M. Assessment of Density Functional Methods for Obtaining Geometries at Conical Intersections in Organic Molecules. *J. Chem. Theory Comput.* **2013**, *9*, 4526−4541.
(14) Zhou, P.; Liu, J.; Han, K.; He, G. The Photoisomerization of 11-*cis*-Retinal Protonated Schiff Base in Gas Phase: Insight from Spin-Flip Density Functional Theory. *J. Comput. Chem.* **2014**, *35*, 109−120.
(15) Nikiforov, A.; Gamez, J. A.; Thiel, W.; Huix-Rotllant, M.; Filatov, M. Assessment of Approximate Computational Methods for Conical Intersections and Branching Plane Vectors in Organic Molecules. *J. Chem. Phys.* **2014**, *141*, 124122.
(16) Valsson, O.; Filippi, C.; Casida, M. E. Regarding the Use and Misuse of Retinal Protonated Schiff Base Photochemistry as a Test Case for Time-Dependent Density-Functional Theory. *J. Chem. Phys.* **2015**, *142*, 144104.
(17) Vreven, T.; Bernardi, F.; Garavelli, M.; Olivucci, M.; Robb, M. A.; Schlegel, H. B. *Ab Initio* Photoisomerization Dynamics of a Simple Retinal Chromophore Model. *J. Am. Chem. Soc.* **1997**, *119*, 12687−12688.
(18) Weingart, O.; Migani, A.; Olivucci, M.; Robb, M. A.; Buss, V.; Hunt, P. Probing the Photochemical Funnel of a Retinal Chromophore Model via Zero-Point Energy Sampling Semiclassical Dynamics. *J. Phys. Chem. A* **2004**, *108*, 4685−4693.
(19) Barbatti, M.; Ruckenbauer, M.; Szymczak, J. J.; Aquino, A. J. A.; Lischka, H. Nonadiabatic Excited-State Dynamics of Polar $\pi$-Systems and Related Model Compounds of Biological Relevance. *Phys. Chem. Chem. Phys.* **2008**, *10*, 482−494.
(20) Szymczak, J. J.; Barbatti, M.; Lischka, H. Mechanism of Ultrafast Photodecay in Restricted Motions in Protonated Schiff Bases: The Pentadieniminium Cation. *J. Chem. Theory Comput.* **2008**, *4*, 1189−1199.
(21) Weingart, O. The Role of HOOP-Modes in the Ultrafast Photo-Isomerization of Retinal Models. *Chem. Phys.* **2008**, *349*, 348−355.
(22) Ishida, T.; Nanbu, S.; Nakamura, H. Nonadiabatic Ab Initio Dynamics of Two Models of Schiff Base Retinal. *J. Phys. Chem. A* **2009**, *113*, 4356−4366.
(23) Malhado, J. P.; Spezia, R.; Hynes, J. T. Dynamical Friction Effects on the Photoisomerization of a Model Protonated Schiff Base in Solution. *J. Phys. Chem. A* **2011**, *115*, 3720−3735.
(24) Klaffki, N.; Weingart, O.; Garavelli, M.; Spohr, E. Sampling Excited State Dynamics: Influence of HOOP Mode Excitations in a Retinal Model. *Phys. Chem. Chem. Phys.* **2012**, *14*, 14299−14305.
(25) Ruckenbauer, M.; Barbatti, M.; Müller, T.; Lischka, H. Nonadiabatic Photodynamics of a Retinal Model in Polar and Nonpolar Environment. *J. Phys. Chem. A* **2013**, *117*, 2790−2799.
(26) Kobayashi, O.; Nanbu, S. Application of Particle-Mesh Ewald Summation to ONIOM Theory. *Chem. Phys.* **2015**, *461*, 47−57.
(27) Gozem, S.; Huntress, M.; Schapiro, I.; Lindh, R.; Granovsky, A. A.; Angeli, C.; Olivucci, M. Dynamic Electron Correlation Effects on the Ground State Potential Energy Surface of a Retinal Chromophore Model. *J. Chem. Theory Comput.* **2012**, *8*, 4069−4080.
(28) Gozem, S.; Krylov, A. I.; Olivucci, M. Conical Intersection and Potential Energy Surface Features of a Model Retinal Chromophore: Comparison of EOM-CC and Multireference Methods. *J. Chem. Theory Comput.* **2013**, *9*, 284−292.
(29) Xu, X.; Gozem, S.; Olivucci, M.; Truhlar, D. G. Combined Self-Consistent-Field and Spin-Flip Tamm-Dancoff Density Functional Approach to Potential Energy Surfaces for Photochemistry. *J. Phys. Chem. Lett.* **2013**, *4*, 253−258.
(30) Huix-Rotllant, M.; Filatov, M.; Gozem, S.; Schapiro, I.; Olivucci, M.; Ferré, N. Assessment of Density Functional Theory for Describing the Correlation Effects on the Ground and Excited State Potential Energy Surfaces of a Retinal Chromophore Model. *J. Chem. Theory Comput.* **2013**, *9*, 3917−3932.
(31) Gozem, S.; Melaccio, F.; Lindh, R.; Krylov, A. I.; Granovsky, A. A.; Angeli, C.; Olivucci, M. Mapping the Excited State Potential Energy Surface of a Retinal Chromophore Model with Multireference and Equation-of-Motion Coupled-Cluster Methods. *J. Chem. Theory Comput.* **2013**, *9*, 4495−4506.
(32) Gozem, S.; Melaccio, F.; Valentini, A.; Filatov, M.; Huix-Rotllant, M.; Ferré, N.; Frutos, L. M.; Angeli, C.; Krylov, A. I.; Granovsky, A. A.; Lindh, R.; Olivucci, M. Shape of Multireference, Equation-of-Motion Coupled-Cluster, and Density Functional Theory Potential Energy Surfaces at a Conical Intersection. *J. Chem. Theory Comput.* **2014**, *10*, 3074−3084.
(33) Schapiro, I.; Neese, F. SORCI for Photochemical and Thermal Reaction Paths: A Benchmark Study. *Comput. Theor. Chem.* **2014**, *1040-1041*, 84−98.
(34) Zen, A.; Coccia, E.; Gozem, S.; Olivucci, M.; Guidoni, L. Quantum Monte Carlo Treatment of the Charge Transfer and Diradical Electronic Character in a Retinal Chromophore Minimal Model. *J. Chem. Theory Comput.* **2015**, *11*, 992−1005.
(35) Serrano-Andrés, L.; Merchán, M. Quantum Chemistry of the Excited State: 2005 Overview. *J. Mol. Struct.: THEOCHEM* **2005**, *729*, 99−108.
(36) Dreuw, A. Quantum Chemical Methods for the Investigation of Photoinitiated Processes in Biological Systems: Theory and Applications. *ChemPhysChem* **2006**, *7*, 2259−2274.
(37) González, L.; Escudero, D.; Serrano-Andrés, L. Progress and Challenges in the Calculation of Electronic Excited States. *ChemPhysChem* **2012**, *13*, 28−51.
(38) Christiansen, O.; Koch, H.; Jørgensen, P. The Second-Order Approximate Coupled Cluster Singles and Doubles Model CC2. *Chem. Phys. Lett.* **1995**, *243*, 409−418.
(39) Furche, F.; Ahlrichs, R.; Hättig, C.; Klopper, W.; Sierka, M.; Weigend, F. Turbomole. *Turbomole. WIREs Comput. Mol. Sci.* **2014**, *4*, 91−100.
(40) Hättig, C.; Weigend, F. CC2 Excitation Energy Calculations on Large Molecules Using the Resolution of the Identity Approximation. *J. Chem. Phys.* **2000**, *113*, 5154−5161.


DOI: 10.1021/acs.jctc.5b00022
*J. Chem. Theory Comput.* 2015, 11, 5758−5781

(41) Köhn, A.; Hättig, C. Analytic Gradients for Excited States in the Coupled-Cluster Model CC2 Employing the Resolution-of-the-Identity Approximation. *J. Chem. Phys.* **2003**, *119*, 5021−5036.
(42) Hättig, C. Structure Optimizations for Excited States with Correlated Second-Order Methods: CC2 and ADC(2). *Adv. Quantum Chem.* **2005**, *50*, 37−60.
(43) Hättig, C.; Köhn, A. Transition Moments and Excited-State First-Order Properties in the Coupled-Cluster Model CC2 Using the Resolution-of-the-Identity Approximation. *J. Chem. Phys.* **2002**, *117*, 6939−6951.
(44) Aidas, K.; Angeli, C.; Bak, K. L.; Bakken, V.; Bast, R.; Boman, L.; Christiansen, O.; Cimiraglia, R.; Coriani, S.; Dahle, P.; Dalskov, E. K.; Ekström, U.; Enevoldsen, T.; Eriksen, J. J.; Ettenhuber, P.; Fernández, B.; Ferrighi, L.; Fliegl, H.; Frediani, L.; Hald, K.; Halkier, A.; Hättig, C.; Heiberg, H.; Helgaker, T.; Hennum, A. F.; Hettema, H.; Hjertenæs, E.; Høst, S.; Høyvik, I.-M.; Iozzi, M. F.; Jansík, B.; Jensen, H. J. A.; Jonsson, D.; Jørgensen, P.; Kauczor, J.; Kirpekar, S.; Kjærgaard, T.; Klopper, W.; Knecht, S.; Kobayashi, R.; Koch, H.; Kongsted, J.; Krapp, A.; Kristensen, K.; Ligabue, A.; Lutnæs, O. B.; Melo, J. I.; Mikkelsen, K. V.; Myhre, R. H.; Neiss, C.; Nielsen, C. B.; Norman, P.; Olsen, J.; Olsen, J. M. H.; Osted, A.; Packer, M. J.; Pawlowski, F.; Pedersen, T. B.; Provasi, P. F.; Reine, S.; Rinkevicius, Z.; Ruden, T. A.; Ruud, K.; Rybkin, V. V.; Sałek, P.; Samson, C. C. M.; Sánchez de Merá, A.; Saue, T.; Sauer, S. P. A.; Schimmelpfennig, B.; Sneskov, K.; Steindal, A. H.; Sylvester-Hvid, K. O.; Taylor, P. R.; Teale, A. M.; Tellgren, E. I.; Tew, D. P.; Thorvaldsen, A. J.; Thøgersen, L.; Vahtras, O.; Watson, M. A.; Wilson, D. J. D.; Ziolkowski, M.; Ågren, H. The Dalton Quantum Chemistry Program System. *WIREs Comput. Mol. Sci.* **2014**, *4*, 269−284.
(45) Stanton, J. F.; Gauss, J.; Harding, M. E.; Szalay, P. G.; Almlöf, J.; Auer, A. A.; Bartlett, R. J.; Benedikt, U.; Berger, C.; Bernholdt, D. E.; Bomble, Y. J.; Cheng, L.; Christiansen, O.; Heckert, M.; Helgaker, T.; Heun, O.; Huber, C.; Jagau, T.-C.; Jensen, H. J. A.; Jonsson, D.; Jørgensen, P.; Jusélius, J.; Klein, K.; Lauderdale, W. J.; Matthews, D. A.; Metzroth, T.; Mitin, A. V.; Mück, L. A.; Olsen, J.; O'Neill, D. P.; Price, D. R.; Prochnow, E.; Puzzarini, C.; Ruud, K.; Schiffmann, F.; Schwalbach, W.; Simmons, C.; Stopkowicz, S.; Tajti, A.; Taylor, P. R.; Vázquez, J.; Wang, F.; Watts, J. D.; van Wüllen, C. *CFOUR*, Coupled-Cluster Techniques for Computational Chemistry, a Quantum-Chemical Program Package. http://www.cfour.de.
(46) Turney, J. M.; Simmonett, A. C.; Parrish, R. M.; Hohenstein, E. G.; Evangelista, F. A.; Fermann, J. T.; Mintz, B. J.; Burns, L. A.; Wilke, J. J.; Abrams, M. L.; Russ, N. J.; Leininger, M. L.; Janssen, C. L.; Seidl, E. T.; Allen, W. D.; Schaefer, H. F.; King, R. A.; Valeev, E. F.; Sherrill, C. D.; Crawford, T. D. Psi4: An Open-Source *Ab Initio* Electronic Structure Program. *WIREs Comput. Mol. Sci.* **2012**, *2*, 556−565.
(47) Werner, H.-J.; Knowles, P. J.; Knizia, G.; Manby, F. R.; Schütz, M. Molpro: A General-Purpose Quantum Chemistry Program Package. *WIREs Comput. Mol. Sci.* **2012**, *2*, 242−253.
(48) van Dam, H. J. J.; de Jong, W. A.; Bylaska, E.; Govind, N.; Kowalski, K.; Straatsma, T. P.; Valiev, M. NWChem: Scalable Parallel Computational Chemistry. *WIREs Comput. Mol. Sci.* **2011**, *1*, 888−894.
(49) Sobolewski, A. L.; Domcke, W.; Hättig, C. Tautomeric Selectivity of the Excited-State Lifetime of Guanine/Cytosine Base Pairs: The Role of Electron-Driven Proton- Transfer Processes. *Proc. Natl. Acad. Sci. U. S. A.* **2005**, *102*, 17903−17906.
(50) Fleig, T.; Knecht, S.; Hättig, C. Quantum-Chemical Investigation of the Structures and Electronic Spectra of the Nucleic Acid Bases at the Coupled Cluster CC2 Level. *J. Phys. Chem. A* **2007**, *111*, 5482−5491.
(51) Falden, H. H.; Falster-Hansen, K. R.; Bak, K. L.; Rettrup, S.; Sauer, S. P. A. Benchmarking Second Order Methods for the Calculation of Vertical Electronic Excitation Energies: Valence and Rydberg States in Polycyclic Aromatic Hydrocarbons. *J. Phys. Chem. A* **2009**, *113*, 11995−12012.
(52) Shemesh, D.; Sobolewski, A. L.; Domcke, W. Efficient Excited-State Deactivation of the Gly-Phe-Ala Tripeptide via an Electron-Driven Proton-Transfer Process. *J. Am. Chem. Soc.* **2009**, *131*, 1374−1375.
(53) Silva-Junior, M. R.; Sauer, S. P. A.; Schreiber, M.; Thiel, W. Basis Set Effects on Coupled Cluster Benchmarks of Electronically Excited States: CC3, CCSDR(3) and CC2. *Mol. Phys.* **2010**, *108*, 453−465.
(54) Goerigk, L.; Grimme, S. Assessment of TD-DFT Methods and of Various Spin Scaled CIS(D) and CC2 Versions for the Treatment of Low-Lying Valence Excitations of Large Organic Dyes. *J. Chem. Phys.* **2010**, *132*, 184103.
(55) Send, R.; Kaila, V. R. I.; Sundholm, D. Benchmarking the Approximate Second-Order Coupled-Cluster Method on Biochromophores. *J. Chem. Theory Comput.* **2011**, *7*, 2473−2484.
(56) Szalay, P. G.; Watson, T.; Perera, A.; Lotrich, V. F.; Bartlett, R. J. Benchmark Studies on the Building Blocks of DNA. 1. Superiority of Coupled Cluster Methods in Describing the Excited States of Nucleobases in the Franck-Condon Region. *J. Phys. Chem. A* **2012**, *116*, 6702−6710.
(57) Sneskov, K.; Christiansen, O. Excited State Coupled Cluster Methods. *WIREs Comput. Mol. Sci.* **2012**, *2*, 566−584.
(58) Winter, N. O. C.; Graf, N. K.; Leutwyler, S.; Hättig, C. Benchmarks for 0−0 Transitions of Aromatic Organic Molecules: DFT/B3LYP, ADC(2), CC2, SOS-CC2 and SCS-CC2 Compared to High-Resolution Gas-Phase Data. *Phys. Chem. Chem. Phys.* **2013**, *15*, 6623−6630.
(59) Delchev, V. B. Excited-State Relaxation Paths of Oxo/Hydroxy and N9H/N7H Tautomers of Guanine: A CC2 Theoretical Study. *J. Mol. Model.* **2013**, *19*, 2299−2308.
(60) Walczak, E.; Szefczyk, B.; Andruniów, T. Geometries and Vertical Excitation Energies in Retinal Analogues Resolved at the CASPT2 Level of Theory: Critical Assessment of the Performance of CASSCF, CC2, and DFT Methods. *J. Chem. Theory Comput.* **2013**, *9*, 4915−4927.
(61) Etinski, M.; Tatchen, J.; Marian, C. M. Thermal and Solvent Effects on the Triplet Formation in Cinnoline. *Phys. Chem. Chem. Phys.* **2014**, *16*, 4740−4751.
(62) Tuna, D.; Sobolewski, A. L.; Domcke, W. Photochemical Mechanisms of Radiationless Deactivation Processes in Urocanic Acid. *J. Phys. Chem. B* **2014**, *118*, 976−985.
(63) Fliegl, H.; Sundholm, D. Coupled-Cluster Calculations of the Lowest 0−0 Bands of the Electronic Excitation Spectrum of Naphthalene. *Phys. Chem. Chem. Phys.* **2014**, *16*, 9859−9865.
(64) Fang, C.; Oruganti, B.; Durbeej, B. How Method-Dependent Are Calculated Differences between Vertical, Adiabatic, and 0−0 Excitation Energies? *J. Phys. Chem. A* **2014**, *118*, 4157−4171.
(65) Benda, Z.; Szalay, P. G. Details of the Excited-State Potential Energy Surfaces of Adenine by Coupled Cluster Techniques. *J. Phys. Chem. A* **2014**, *118*, 6197−6207.
(66) Kánnár, D.; Szalay, P. G. Benchmarking Coupled Cluster Methods on Valence Singlet Excited States. *J. Chem. Theory Comput.* **2014**, *10*, 3757−3765.
(67) Kánnár, D.; Szalay, P. G. Benchmarking Coupled Cluster Methods on Singlet Excited States of Nucleobases. *J. Mol. Model.* **2014**, *20*, 2503.
(68) Gromov, E. V. Unveiling the Mechanism of Photoinduced Isomerization of the Photoactive Yellow Protein (PYP) Chromophore. *J. Chem. Phys.* **2014**, *141*, 224308.
(69) Schwabe, T.; Beerepoot, M. T. P.; Olsen, J. M. H.; Kongsted, J. Analysis of Computational Models for an Accurate Study of Electronic Excitations in GFP. *Phys. Chem. Chem. Phys.* **2015**, *17*, 2582−2588.
(70) Kopec, S.; Ottiger, P.; Leutwyler, S.; Köppel, H. Analysis of the $S_2 \leftarrow S_0$ Vibronic Spectrum of the *ortho*-Cyanophenol Dimer Using a Multimode Vibronic Coupling Approach. *J. Chem. Phys.* **2015**, *142*, 084308.
(71) Send, R.; Suomivuori, C.-M.; Kaila, V. R. I.; Sundholm, D. Coupled-Cluster Studies of Extensive Green Fluorescent Protein Models Using the Reduced Virtual Space Approach. *J. Phys. Chem. B* **2015**, *119*, 2933−2945.
(72) Crespo-Otero, R.; Kungwan, N.; Barbatti, M. Stepwise Double Excited-State Proton Transfer Is Not Possible in 7-Azaindole Dimer. *Chem. Sci.* **2015**, *6*, 5762−5767.
(73) Balmer, F. A.; Trachsel, M. A.; van der Avoird, A.; Leutwyler, S. The Elusive $S_2$ State, the $S_1/S_2$ Splitting, and the Excimer States of the Benzene Dimer. *J. Chem. Phys.* **2015**, *142*, 234306.


DOI: 10.1021/acs.jctc.5b00022
*J. Chem. Theory Comput.* 2015, 11, 5758−5781

(74) Guiglion, P.; Zwijnenburg, M. A. Contrasting the Optical Properties of the Different Isomers of Oligophenylene. *Phys. Chem. Chem. Phys.* **2015**, *17*, 17854−17863.
(75) Laurent, A. D.; Blondel, A.; Jacquemin, D. Choosing an Atomic Basis Set for TD-DFT, SOPPA, ADC(2), CIS(D), CC2 and EOM-CCSD Calculations of Low-Lying Excited States of Organic Dyes. *Theor. Chem. Acc.* **2015**, *134*, 76.
(76) Jacquemin, D.; Duchemin, I.; Blase, X. 0−0 Energies Using Hybrid Schemes: Benchmarks of TD-DFT, CIS(D), ADC(2), CC2, and BSE/*GW* formalisms for 80 Real-Life Compounds. *J. Chem. Theory Comput.* **2015**, *11* (11), 5340−5359.
(77) Send, R.; Kaila, V. R. I.; Sundholm, D. Reduction of the Virtual Space for Coupled-Cluster Excitation Energies of Large Molecules and Embedded Systems. *J. Chem. Phys.* **2011**, *134*, 214114.
(78) Helmich, B.; Hättig, C. A Pair Natural Orbital Implementation of the Coupled Cluster Model CC2 for Excitation Energies. *J. Chem. Phys.* **2013**, *139*, 084114.
(79) Hohenstein, E. G.; Kokkila, S. I. L.; Parrish, R. M.; Martínez, T. J. Quartic Scaling Second-Order Approximate Coupled Cluster Singles and Doubles via Tensor Hypercontraction: THC-CC2. *J. Chem. Phys.* **2013**, *138*, 124111.
(80) Hohenstein, E. G.; Kokkila, S. I. L.; Parrish, R. M.; Martínez, T. J. Tensor Hypercontraction Equation-of-Motion Second-Order Approximate Coupled Cluster: Electronic Excitation Energies in $O(N^4)$ Time. *J. Phys. Chem. B* **2013**, *117*, 12972−12978.
(81) Ledermüller, K.; Schütz, M. Local CC2 Response Method Based on the Laplace Transform: Analytic Energy Gradients for Ground and Excited States. *J. Chem. Phys.* **2014**, *140*, 164113.
(82) Schirmer, J. Beyond the Random-Phase Approximation: A New Approximation Scheme for the Polarization Propagator. *Phys. Rev. A: At., Mol., Opt. Phys.* **1982**, *26*, 2395−2416.
(83) Trofimov, A. B.; Schirmer, J. An Efficient Polarization Propagator Approach to Valence Electron Excitation Spectra. *J. Phys. B: At., Mol. Opt. Phys.* **1995**, *28*, 2299−2324.
(84) Krylov, A. I.; Gill, P. M. W. Q-Chem: An Engine for Innovation. *WIREs Comput. Mol. Sci.* **2013**, *3*, 317−326.
(85) Shao, Y.; Gan, Z.; Epifanovsky, E.; Gilbert, A. T.; Wormit, M.; Kussmann, J.; Lange, A. W.; Behn, A.; Deng, J.; Feng, X.; Ghosh, D.; Goldey, M.; Horn, P. R.; Jacobson, L. D.; Kaliman, I.; Khaliullin, R. Z.; Kuś, T.; Landau, A.; Liu, J.; Proynov, E. I.; Rhee, Y. M.; Richard, R. M.; Rohrdanz, M. A.; Steele, R. P.; Sundstrom, E. J.; Woodcock, H. L.; Zimmerman, P. M.; Zuev, D.; Albrecht, B.; Alguire, E.; Austin, B.; Beran, G. J. O.; Bernard, Y. A.; Berquist, E.; Brandhorst, K.; Bravaya, K. B.; Brown, S. T.; Casanova, D.; Chang, C.-M.; Chen, Y.; Chien, S. H.; Closser, K. D.; Crittenden, D. L.; Diedenhofen, M.; DiStasio, R. A.; Do, H.; Dutoi, A. D.; Edgar, R. G.; Fatehi, S.; Fusti-Molnar, L.; Ghysels, A.; Golubeva-Zadorozhnaya, A.; Gomes, J.; Hanson-Heine, M. W.; Harbach, P. H. P.; Hauser, A. W.; Hohenstein, E. G.; Holden, Z. C.; Jagau, T.-C.; Ji, H.; Kaduk, B.; Khistyaev, K.; Kim, J.; Kim, J.; King, R. A.; Klunzinger, P.; Kosenkov, D.; Kowalczyk, T.; Krauter, C. M.; Lao, K. U.; Laurent, A.; Lawler, K. V.; Levchenko, S. V.; Lin, C. Y.; Liu, F.; Livshits, E.; Lochan, R. C.; Luenser, A.; Manohar, P.; Manzer, S. F.; Mao, S.-P.; Mardirossian, N.; Marenich, A. V.; Maurer, S. A.; Mayhall, N. J.; Neuscamman, E.; Oana, C. M.; Olivares-Amaya, R.; O'Neill, D. P.; Parkhill, J. A.; Perrine, T. M.; Peverati, R.; Prociuk, A.; Rehn, D. R.; Rosta, E.; Russ, N. J.; Sharada, S. M.; Sharma, S.; Small, D. W.; Sodt, A.; Stein, T.; Stück, D.; Su, Y.-C.; Thom, A. J.; Tsuchimochi, T.; Vanovschi, V.; Vogt, L.; Vydrov, O.; Wang, T.; Watson, M. A.; Wenzel, J.; White, A.; Williams, C. F.; Yang, J.; Yeganeh, S.; Yost, S. R.; You, Z.-Q.; Zhang, I. Y.; Zhang, X.; Zhao, Y.; Brooks, B. R.; Chan, G. K.; Chipman, D. M.; Cramer, C. J.; Goddard, W. A.; Gordon, M. S.; Hehre, W. J.; Klamt, A.; Schaefer, H. F.; Schmidt, M. W.; Sherrill, C. D.; Truhlar, D. G.; Warshel, A.; Xu, X.; Aspuru-Guzik, A.; Baer, R.; Bell, A. T.; Besley, N. A.; Chai, J.-D.; Dreuw, A.; Dunietz, B. D.; Furlani, T. R.; Gwaltney, S. R.; Hsu, C.-P.; Jung, Y.; Kong, J.; Lambrecht, D. S.; Liang, W.; Ochsenfeld, C.; Rassolov, V. A.; Slipchenko, L. V.; Subotnik, J. E.; Van Voorhis, T.; Herbert, J. M.; Krylov, A. I.; Gill, P. M.; Head-Gordon, M. Advances in Molecular Quantum Chemistry Contained in the Q-Chem 4 Program Package. *Mol. Phys.* **2015**, *113*, 184−215.
(86) Wormit, M.; Rehn, D. R.; Harbach, P. H. P.; Wenzel, J.; Krauter, C. M.; Epifanovsky, E.; Dreuw, A. Investigating Excited Electronic States Using the Algebraic Diagrammatic Construction (ADC) Approach of the Polarization Propagator. *Mol. Phys.* **2014**, *112*, 774−784.
(87) Dreuw, A.; Wormit, M. The Algebraic Diagrammatic Construction Scheme for the Polarization Propagator for the Calculation of Excited States. *WIREs Comput. Mol. Sci.* **2015**, *5*, 82−95.
(88) Harbach, P. H. P.; Wormit, M.; Dreuw, A. The Third-Order Algebraic Diagrammatic Construction Method (ADC(3)) for the Polarization Propagator for Closed-Shell Molecules: Efficient Implementation and Benchmarking. *J. Chem. Phys.* **2014**, *141*, 064113.
(89) Helmich, B.; Hättig, C. A Pair Natural Orbital Based Implementation of ADC(2)-x: Perspectives and Challenges for Response Methods for Singly and Doubly Excited States in Large Molecules. *Comput. Theor. Chem.* **2014**, *1040-1041*, 35−44.
(90) Schütz, M. Oscillator Strengths, First-Order Properties, and Nuclear Gradients for Local ADC(2). *J. Chem. Phys.* **2015**, *142*, 214103.
(91) Lefrancois, D.; Wormit, M.; Dreuw, A. Adapting Algebraic Diagrammatic Construction Schemes for the Polarization Propagator to Problems with Multi-Reference Electronic Ground States Exploiting the Spin-Flip Ansatz. *J. Chem. Phys.* **2015**, *143*, 124107.
(92) Pabst, M.; Köhn, A.; Gauss, J.; Stanton, J. F. A Worrisome Failure of the CC2 Coupled-Cluster Method when Applied to Ozone. *Chem. Phys. Lett.* **2010**, *495*, 135−140.
(93) Aquino, A. J. A.; Nachtigallova, D.; Hobza, P.; Truhlar, D. G.; Hättig, C.; Lischka, H. The Charge-Transfer States in a Stacked Nucleobase Dimer Complex: A Benchmark Study. *J. Comput. Chem.* **2011**, *32*, 1217−1227.
(94) Shemesh, D.; Sobolewski, A. L.; Domcke, W. Role of Excited-State Hydrogen Detachment and Hydrogen-Transfer Processes for the Excited-State Deactivation of an Aromatic Dipeptide: N-Acetyl Tryptophan Methyl Amide. *Phys. Chem. Chem. Phys.* **2010**, *12*, 4899−4905.
(95) Panda, A. N.; Plasser, F.; Aquino, A. J. A.; Burghardt, I.; Lischka, H. Electronically Excited States in Poly(*p*-phenylenevinylene): Vertical Excitations and Torsional Potentials from High-Level Ab Initio Calculations. *J. Phys. Chem. A* **2013**, *117*, 2181−2189.
(96) Tuna, D.; Sobolewski, A. L.; Domcke, W. Mechanisms of Ultrafast Excited-State Deactivation in Adenosine. *J. Phys. Chem. A* **2014**, *118*, 122−127.
(97) Tuna, D.; Došlić, N.; Mališ, M.; Sobolewski, A. L.; Domcke, W. Mechanisms of Photostability in Kynurenines: A Joint Electronic-Structure and Dynamics Study. *J. Phys. Chem. B* **2015**, *119*, 2112−2124.
(98) Liu, X.; Sobolewski, A. L.; Domcke, W. Photoinduced Oxidation of Water in the Pyridine−Water Complex: Comparison of the Singlet and Triplet Photochemistries. *J. Phys. Chem. A* **2014**, *118*, 7788−7795.
(99) Mewes, J.-M.; Jovanović, V.; Marian, C.; Dreuw, A. On the Molecular Mechanism of Non-Radiative Decay of Nitrobenzene and the Unforeseen Challenges This Simple Molecule Holds for Electronic Structure Theory. *Phys. Chem. Chem. Phys.* **2014**, *16*, 12393−12406.
(100) Szabla, R.; Šponer, J. E.; Šponer, J.; Sobolewski, A. L.; Góra, R. W. Solvent Effects on the Photochemistry of 4-Aminoimidazole-5-carbonitrile, a Prebiotically Plausible Precursor of Purines. *Phys. Chem. Chem. Phys.* **2014**, *16*, 17617−17626.
(101) Kochman, M. A.; Tajti, A.; Morrison, C. A.; Miller, R. J. D. Early Events in the Nonadiabatic Relaxation Dynamics of 4-(*N*,*N*-Dimethylamino)benzonitrile. *J. Chem. Theory Comput.* **2015**, *11*, 1118−1128.
(102) Huang, J.; Du, L.; Hu, D.; Lan, Z. Theoretical Analysis of Excited States and Energy Transfer Mechanism in Conjugated Dendrimers. *J. Comput. Chem.* **2015**, *36*, 151−163.
(103) Gámiz-Hernández, A.-P.; Magomedov, A.; Hummer, G.; Kaila, V. R. I. Linear Energy Relationships in Ground State Proton Transfer and Excited State Proton-Coupled Electron Transfer. *J. Phys. Chem. B* **2015**, *119*, 2611−2619.
(104) Barbatti, M.; Lischka, H. Why Water Makes 2-Aminopurine Fluorescent? *Phys. Chem. Chem. Phys.* **2015**, *17*, 15452−15459.
(105) Karsili, T. N. V.; Tuna, D.; Ehrmaier, J.; Domcke, W. Photoinduced Water Splitting via Benzoquinone and Semiquinone


DOI: 10.1021/acs.jctc.5b00022
*J. Chem. Theory Comput.* 2015, 11, 5758−5781

Sensitisation. *Phys. Chem. Chem. Phys.* **2015**, DOI: 10.1039/C5CP03831F.
(106) Liu, W.; Lunkenheimer, B.; Settels, V.; Engels, B.; Fink, R. F.; Köhn, A. A General Ansatz for Constructing Quasi-Diabatic States in Electronically Excited Aggregated Systems. *J. Chem. Phys.* **2015**, *143*, 084106.
(107) Plasser, F.; Aquino, A. J. A.; Hase, W. L.; Lischka, H. UV Absorption Spectrum of Alternating DNA Duplexes. Analysis of Excitonic and Charge Transfer Interactions. *J. Phys. Chem. A* **2012**, *116*, 11151−11160.
(108) Plasser, F.; Lischka, H. Electronic Excitation and Structural Relaxation of the Adenine Dinucleotide in Gas Phase and Solution. *Photochem. Photobiol. Sci.* **2013**, *12*, 1440−1452.
(109) Spata, V. A.; Matsika, S. Role of Excitonic Coupling and Charge-Transfer States in the Absorption and CD Spectra of Adenine-Based Oligonucleotides Investigated through QM/MM Simulations. *J. Phys. Chem. A* **2014**, *118*, 12021−12030.
(110) Plasser, F.; Crespo-Otero, R.; Pederzoli, M.; Pittner, J.; Lischka, H.; Barbatti, M. Surface Hopping Dynamics with Correlated Single-Reference Methods: 9H-Adenine as a Case Study. *J. Chem. Theory Comput.* **2014**, *10*, 1395−1405.
(111) Du, L.; Lan, Z. An On-the-Fly Surface-Hopping Program JADE for Nonadiabatic Molecular Dynamics of Polyatomic Systems: Implementation and Applications. *J. Chem. Theory Comput.* **2015**, *11*, 1360−1374.
(112) Prlj, A.; Curchod, B. F. E.; Corminboeuf, C. Excited State Dynamics of Thiophene and Bithiophene: New Insights into Theoretically Challenging Systems. *Phys. Chem. Chem. Phys.* **2015**, *17*, 14719−14730.
(113) Sapunar, M.; Ponzi, A.; Chaiwongwattana, S.; Mališ, M.; Prlj, A.; Decleva, P.; Došlić, N. Timescales of N−H Bond Dissociation in Pyrrole: A Nonadiabatic Dynamics Study. *Phys. Chem. Chem. Phys.* **2015**, *17*, 19012−19020.
(114) Kungwan, N.; Kerdpol, K.; Daengngern, R.; Hannongbua, S.; Barbatti, M. Effects of the Second Hydration Shell on Excited-State Multiple Proton Transfer: Dynamics Simulations of 7-Azaindole: $(H_2O)_{1\text{-}5}$ Clusters in the Gas Phase. *Theor. Chem. Acc.* **2014**, *133*, 1480.
(115) Barbatti, M. Photorelaxation Induced by Water−Chromophore Electron Transfer. *J. Am. Chem. Soc.* **2014**, *136*, 10246−10249.
(116) Chaiwongwattana, S.; Sapunar, M.; Ponzi, A.; Decleva, P.; Došlić, N. Exploration of Excited State Deactivation Pathways of Adenine Monohydrates. *J. Phys. Chem. A* **2015**, *119*, 10637−10644.
(117) Starcke, J. H.; Wormit, M.; Dreuw, A. Nature of the Lowest Excited States of Neutral Polyenyl Radicals and Polyene Radical Cations. *J. Chem. Phys.* **2009**, *131*, 144311.
(118) Saitow, M.; Mochizuki, Y. Excited State Calculation for Free-Base and Metalloporphyrins with the Partially Renormalized Polarization Propagator Approach. *Chem. Phys. Lett.* **2012**, *525-526*, 144−149.
(119) Lunkenheimer, B.; Köhn, A. Solvent Effects on Electronically Excited States Using the Conductor-Like Screening Model and the Second-Order Correlated Method ADC(2). *J. Chem. Theory Comput.* **2013**, *9*, 977−994.
(120) Li, H.; Nieman, R.; Aquino, A. J. A.; Lischka, H.; Tretiak, S. Comparison of LC−TDDFT and ADC(2) Methods in Computations of Bright and Charge Transfer States in Stacked Oligothiophenes. *J. Chem. Theory Comput.* **2014**, *10*, 3280−3289.
(121) Wenzel, J.; Wormit, M.; Dreuw, A. Calculating Core-Level Excitations and X-Ray Absorption Spectra of Medium-Sized Closed-Shell Molecules with the Algebraic-Diagrammatic Construction Scheme for the Polarization Propagator. *J. Comput. Chem.* **2014**, *35*, 1900−1915.
(122) Cardozo, T. M.; Aquino, A. J. A.; Barbatti, M., Jr.; Borges, I.; Lischka, H. Absorption and Fluorescence Spectra of Poly(p-phenylenevinylene) (PPV) Oligomers: An *Ab Initio* Simulation. *J. Phys. Chem. A* **2015**, *119*, 1787−1795.
(123) Plekan, O.; Feyer, V.; Richter, R.; Moise, A.; Coreno, M.; Prince, K. C.; Zaytseva, I. L.; Moskovskaya, T. E.; Soshnikov, D. Y.; Trofimov, A. B. X-Ray Spectroscopy of Heterocyclic Biochemicals: Xanthine, Hypoxanthine, and Caffeine. *J. Phys. Chem. A* **2012**, *116*, 5653−5664.
(124) Wenzel, J.; Wormit, M.; Dreuw, A. Calculating X-Ray Absorption Spectra of Open-Shell Molecules with the Unrestricted Algebraic-Diagrammatic Construction Scheme for the Polarization Propagator. *J. Chem. Theory Comput.* **2014**, *10*, 4583−4598.
(125) Ruberti, M.; Yun, R.; Gokhberg, K.; Kopelke, S.; Cederbaum, L. S.; Tarantelli, F.; Averbukh, V. Total Photoionization Cross−Sections of Excited Electronic States by the Algebraic Diagrammatic Construction-Stieltjes−Lanczos Method. *J. Chem. Phys.* **2014**, *140*, 184107.
(126) Knippenberg, S.; Eisenbrandt, P.; Šištík, L.; Slavíček, P.; Dreuw, A. Simulation of Photoelectron Spectra Using the Reflection Principle in Combination with Unrestricted Excitation ADC(2) to Assess the Accuracy of Excited-State Calculations. *ChemPhysChem* **2011**, *12*, 3180−3191.
(127) Shojaei, S. H. R.; Morini, F.; Deleuze, M. S. Valence One-Electron and Shake-Up Ionization Bands of Fluorene, Carbazole and Dibenzofuran. *Chem. Phys.* **2013**, *417*, 17−25.
(128) Mewes, J.-M.; You, Z.-Q.; Wormit, M.; Kriesche, T.; Herbert, J. M. J. M.; Dreuw, A. Experimental Benchmark Data and Systematic Evaluation of Two *a Posteriori,* Polarizable-Continuum Corrections for Vertical Excitation Energies in Solution. *J. Phys. Chem. A* **2015**, *119*, 5446−5464.
(129) Grimme, S. Improved Second-Order Møller−Plesset Perturbation Theory by Separate Scaling of Parallel- and Antiparallel-Spin Pair Correlation Energies. *J. Chem. Phys.* **2003**, *118*, 9095−9102.
(130) Jung, Y.; Lochan, R. C.; Dutoi, A. D.; Head-Gordon, M. Scaled Opposite−Spin Second Order Møller-Plesset Correlation Energy: An Economical Electronic Structure Method. *J. Chem. Phys.* **2004**, *121*, 9793−9802.
(131) Hellweg, A.; Grün, S.; Hättig, C. Benchmarking the Performance of Spin-Component Scaled CC2 in Ground and Electronically Excited States. *Phys. Chem. Chem. Phys.* **2008**, *10*, 4119−4127.
(132) Krauter, C. M.; Pernpointner, M.; Dreuw, A. Application of the Scaled-Opposite-Spin Approximation to Algebraic Diagrammatic Construction Schemes of Second Order. *J. Chem. Phys.* **2013**, *138*, 044107.
(133) Grimme, S.; Goerigk, L.; Fink, R. F. Spin-Component-Scaled Electron Correlation Methods. *WIREs Comput. Mol. Sci.* **2012**, *2*, 886−906.
(134) Sicilia, F.; Blancafort, L.; Bearpark, M. J.; Robb, M. A. New Algorithms for Optimizing and Linking Conical Intersection Points. *J. Chem. Theory Comput.* **2008**, *4*, 257−266.
(135) Nenov, A.; de Vivie-Riedle, R. Conical Intersection Seams in Polyenes Derived from Their Chemical Composition. *J. Chem. Phys.* **2012**, *137*, 074101.
(136) Mori, T.; Martínez, T. J. Exploring the Conical Intersection Seam: The Seam Space Nudged Elastic Band Method. *J. Chem. Theory Comput.* **2013**, *9*, 1155−1163.
(137) Blancafort, L. Photochemistry and Photophysics at Extended Seams of Conical Intersection. *ChemPhysChem* **2014**, *15*, 3166−3181.
(138) Robb, M. A.; Bernardi, F.; Olivucci, M. Conical Intersections as a Mechanistic Feature of Organic Photochemistry. *Pure Appl. Chem.* **1995**, *67*, 783−789.
(139) Bernardi, F.; Olivucci, M.; Robb, M. A. Potential Energy Surface Crossings in Organic Photochemistry. *Chem. Soc. Rev.* **1996**, *25*, 321−328.
(140) *Conical Intersections: Electronic Structure, Dynamics & Spectroscopy*; Domcke, W., Yarkony, D. R., Köppel, H., Eds.; World Scientific Publishing, Singapore, 2004.
(141) Levine, B. G.; Martínez, T. J. Isomerization Through Conical Intersections. *Annu. Rev. Phys. Chem.* **2007**, *58*, 613−634.
(142) *Conical Intersections: Theory, Computation and Experiment*; Domcke, W., Yarkony, D. R., Köppel, H., Eds.; World Scientific Publishing, Singapore, 2011.
(143) Matsika, S.; Krause, P. Nonadiabatic Events and Conical Intersections. *Annu. Rev. Phys. Chem.* **2011**, *62*, 621−643.
(144) Domcke, W.; Yarkony, D. R. Role of Conical Intersections in Molecular Spectroscopy and Photoinduced Chemical Dynamics. *Annu. Rev. Phys. Chem.* **2012**, *63*, 325−352.


DOI: 10.1021/acs.jctc.5b00022
*J. Chem. Theory Comput.* 2015, 11, 5758−5781

(145) Yarkony, D. R. Nonadiabatic Quantum Chemistry—Past, Present, and Future. *Chem. Rev.* **2012**, *112*, 481−498.
(146) Levine, B. G.; Ko, C.; Quenneville, J.; Martínez, T. J. Conical Intersections and Double Excitations in Time-Dependent Density Functional Theory. *Mol. Phys.* **2006**, *104*, 1039−1051.
(147) Köhn, A.; Tajti, A. Can Coupled-Cluster Theory Treat Conical Intersections? *J. Chem. Phys.* **2007**, *127*, 044105.
(148) Levine, B. G.; Coe, J. D.; Martínez, T. J. Optimizing Conical Intersections without Derivative Coupling Vectors: Application to Multistate Multireference Second-Order Perturbation Theory (MS-CASPT2). *J. Phys. Chem. B* **2008**, *112*, 405−413.
(149) Schirmer, J.; Trofimov, A. A. Intermediate State Representation Approach to Physical Properties of Electronically Excited Molecules. *J. Chem. Phys.* **2004**, *120*, 11449.
(150) *TURBOMOLE*, V6.6; TURBOMOLE GmbH: Karlsruhe, Germany, 2014. http://www.turbomole.com.
(151) Trofimov, A. B.; Stelter, G.; Schirmer, J. Electron Excitation Energies Using a Consistent Third-Order Propagator Approach: Comparison with Full Configuration Interaction and Coupled Cluster Results. *J. Chem. Phys.* **2002**, *117*, 6402−6410.
(152) Frisch, M. J.; Trucks, G. W.; Schlegel, H. B.; Scuseria, G. E.; Robb, M. A.; Cheeseman, J. R.; Montgomery, J. A., Jr.; Vreven, T.; Kudin, K. N.; Burant, J. C.; Millam, J. M.; Iyengar, S. S.; Tomasi, J.; Barone, V.; Mennucci, B.; Cossi, M.; Scalmani, G.; Rega, N.; Petersson, G. A.; Nakatsuji, H.; Hada, M.; Ehara, M.; Toyota, K.; Fukuda, R.; Hasegawa, J.; Ishida, M.; Nakajima, T.; Honda, Y.; Kitao, O.; Nakai, H.; Klene, M.; Li, X.; Knox, J. E.; Hratchian, H. P.; Cross, J. B.; Bakken, V.; Adamo, C.; Jaramillo, J.; Gomperts, R.; Stratmann, R. E.; Yazyev, O.; Austin, A. J.; Cammi, R.; Pomelli, C.; Ochterski, J. W.; Ayala, P. Y.; Morokuma, K.; Voth, G. A.; Salvador, P.; Dannenberg, J. J.; Zakrzewski, V. G.; Dapprich, S.; Daniels, A. D.; Strain, M. C.; Farkas, O.; Malick, D. K.; Rabuck, A. D.; Raghavachari, K.; Foresman, J. B.; Ortiz, J. V.; Cui, Q.; Baboul, A. G.; Clifford, S.; Cioslowski, J.; Stefanov, B. B.; Liu, G.; Liashenko, A.; Piskorz, P.; Komaromi, I.; Martin, R. L.; Fox, D. J.; Keith, T.; Al-Laham, M. A.; Peng, C. Y.; Nanayakkara, A.; Challacombe, M.; Gill, P. M. W.; Johnson, B.; Chen, W.; Wong, M. W.; Gonzalez, C.; Pople, J. A. *Gaussian 03*, revision E.01; Gaussian, Inc.: Wallingford, CT, 2003.
(153) Lischka, H.; Shepard, R.; Shavitt, I.; Pitzer, R. M.; Dallos, M.; Müller, T.; Szalay, P. G.; Brown, F. B.; Ahlrichs, R.; Böhm, H. J.; Chang, A.; Comeau, D. C.; Gdanitz, R.; Dachsel, H.; Ehrhardt, C.; Ernzerhof, M.; Höchtl, P.; Irle, S.; Kedziora, G.; Kovar, T.; Parasuk, V.; Pepper, M. J. M.; Scharf, P.; Schiffer, H.; Schindler, M.; Schüler, M.; Seth, M.; Stahlberg, E. A.; Zhao, J.-G.; Yabushita, S.; Zhang, Z.; Barbatti, M.; Matsika, S.; Schuurmann, M.; Yarkony, D. R.; Brozell, S. R.; Beck, E. V.; Blaudeau, J.-P.; Ruckenbauer, M.; Sellner, B.; Plasser, F.; Szymczak, J. J. *COLUMBUS*, an ab initio electronic structure program, release 7.0, 2012.
(154) Yarkony, D. R. On the Adiabatic to Diabatic States Transformation Near Intersections of Conical Intersections. *J. Chem. Phys.* **2000**, *112*, 2111−2120.
(155) Yarkony, D. R. Nuclear Dynamics Near Conical Intersections in the Adiabatic Representation: I. The Effects of Local Topography on Interstate Transitions. *J. Chem. Phys.* **2001**, *114*, 2601−2613.
(156) Herzberg, G.; Longuet-Higgins, H. C. Intersection of Potential Energy Surfaces in Polyatomic Molecules. *Discuss. Faraday Soc.* **1963**, *35*, 77−82.
(157) Atchity, G. J.; Xantheas, S. S.; Ruedenberg, K. Potential Energy Surfaces Near Intersections. *J. Chem. Phys.* **1991**, *95*, 1862−1876.
(158) Janssen, C. L.; Nielsen, I. M. B. New Diagnostics for Coupled-Cluster and Møller−Plesset Perturbation Theory. *Chem. Phys. Lett.* **1998**, *290*, 423−430.
(159) Nielsen, I. M. B.; Janssen, C. L. Double-Substitution-Based Diagnostics for Coupled-Cluster and Møller−Plesset Perturbation Theory. *Chem. Phys. Lett.* **1999**, *310*, 568−576.
(160) Thiel, W. Semiempirical Quantum-Chemical Methods. *WIREs Comput. Mol. Sci.* **2014**, *4*, 145−157.
(161) Mališ, M.; Loquais, Y.; Gloaguen, E.; Jouvet, C.; Brenner, V.; Mons, M.; Ljubíc, I.; Došlić, N. Non-Radiative Relaxation of UV Photoexcited Phenylalanine Residues: Probing the Role of Conical Intersections by Chemical Substitution. *Phys. Chem. Chem. Phys.* **2014**, *16*, 2285−2288.
(162) Maeda, S.; Ohno, K.; Morokuma, K. Updated Branching Plane for Finding Conical Intersections without Coupling Derivative Vectors. *J. Chem. Theory Comput.* **2010**, *6*, 1538−1545.
(163) Christiansen, O. First-Order Nonadiabatic Coupling Matrix Elements Using Coupled Cluster Methods. I. Theory. *J. Chem. Phys.* **1999**, *110*, 711−723.
(164) Schreiber, M.; Silva-Junior, M. R.; Sauer, S. P. A.; Thiel, W. Benchmarks for Electronically Excited States: CASPT2, CC2, CCSD, and CC3. *J. Chem. Phys.* **2008**, *128*, 134110.


DOI: 10.1021/acs.jctc.5b00022
*J. Chem. Theory Comput.* 2015, 11, 5758−5781